GREEN SYNTHESIS OF IRON OXIDE FOR PHOTOCATALYTIC DEGRADATION OF ORGANIC DYE

CHANG VHUI TAO

A project report submitted in partial fulfilment of the requirements for the award of Bachelor of Engineering (Honours) Chemical Engineering

Lee Kong Chian Faculty of Engineering and Science
Universiti Tunku Abdul Rahman

April 2019

DECLARATION

I hereby declare that this project report is based on my original work except for citations and quotations which have been duly acknowledged. I also declare that it has not been previously and concurrently submitted for any other degree or award at UTAR or other institutions.

Signature   :   _____

Name   :   _____

ID No.   :   _____

Date   :   _____

APPROVAL FOR SUBMISSION

I certify that this project report entitled **"GREEN SYNTHESIS OF IRON OXIDE FOR PHOTOCATALYTIC DEGRADATION OF ORGANIC DYE"** was prepared by **CHANG VHUI TAO** has met the required standard for submission in partial fulfilment of the requirements for the award of Bachelor of Engineering (Hons.) Chemical Engineering at Universiti Tunku Abdul Rahman.

Approved by,

Signature   :

Supervisor   :

Date   :

Signature   :

Co-Supervisor :

Date   :

ACKNOWLEDGEMENTS

I would like to thank everyone who had contributed to the successful completion of this project. I would like to express my gratitude to my research supervisor, Dr. Pang Yean Ling for his invaluable advice, guidance and his enormous patience throughout the development of the research.

In addition, I would also like to express my gratitude to my loving parents and friends who had helped and given me encouragement to complete this project. I would not resolve the problems which I faced during my research without their cooperation.

ABSTRACT

Pure iron oxide, eggshell particles and iron oxide distributed on eggshell particles were used as photocatalysts for photocatalytic degradation of Congo red. The conventional synthesis method by using toxic chemicals to produce iron oxide would cause environmental pollution. Thus, green synthesis method had been investigated based on the principle of green chemistry which involved the design of chemical products and processes that could reduce or eliminate the generation of hazardous substances. Green synthesised pure iron oxide, eggshell particles and iron oxide distributed on eggshell particles were then characterised by using X-ray diffraction (XRD), Fourier-transform infrared spectroscopy (FTIR), scanning electron microscopy coupled with energy dispersive X-ray (SEM-EDX) and thermogravimetric analysis (TGA). Iron oxide was successfully being synthesised by using iron nitrate nanohydrate $(Fe(NO_3)_3 \cdot 9H_2O)$ solution with the addition of orange peel extract. SEM analysis revealed that the morphology of iron oxide was mostly shown in spherical shape with average diameter in range from 0.1-1.0 μm. Iron oxide distributed on eggshell particles showed a higher catalytic activity, which might due to the high porosity of the eggshell particles. There were several parameters had been studied including initial dye concentration (10-50 ppm), catalyst dosage (0.5-2.5 g/L) and solution pH (3-11). The photocatalytic degradation efficiency was increased with decreasing initial dye concentration, increasing catalyst dosage and decreasing solution pH. The highest photocatalytic degradation efficiency of 96% could be achieved at initial dye concentration of 10 ppm, catalyst dosage of 2.5 g/L and solution pH of 3. Furthermore, response surface methodology (RSM) had been used to determine the optimum condition of the photocatalytic degradation of Congo red. The optimum condition was found at initial dye concentration of 20.422 ppm, catalyst dosage of 2.498 g/L and solution pH of 3. It could be concluded that iron oxide distributed on eggshell particles is potentially being used in wastewater treatment application.

TABLE OF CONTENTS

CHAPTER

LIST OF TABLES

LIST OF FIGURES

LIST OF SYMBOLS / ABBREVIATIONS

Br_2	bromine
C	carbon
Ca	calcium
$CaCO_3$	calcium carbonate
$Ca(OH)_2$	calcium hydroxide
Cl_2	chlorine
ClO_2	chlorine dioxide
CO_3^{2-}	carbonate ion
D_C	crystalline size
d	the interplanar spacing generating the diffraction
F_2	fluorine
Fe	iron
Fe^{2+}	ferrous ions
Fe^{3+}	ferric ions
FeO^{2+}	ferryl ions
Fe_2O_3	iron oxide
Fe_3O_4	magnetite
$Fe(NO_3)_3 \cdot 9H_2O$	iron(III) nitrate nanohydrate
$Fe(OH)_2$	iron(II) hydroxide
H_2O	water
H_2O_2	hydrogen peroxide
$H_3O_2^+$	oxonimum ion
HCl	hydrochloric acid
$HClO$	hypochlorous acid
K	shape factor, 0.9
$KMnO_4$	potassium permanganate
$NaOH$	sodium hydroxide
n	integer
O	atomic oxygen
O_2	oxygen
O_3	ozone
$\cdot OH$	hydroxyl radial

$\cdot O_2H$	perhydroxyl radicals
R^2	determination coefficient
TiO_2	titanium dioxide
x_1	initial dye concentration
x_2	catalyst dosage
x_3	solution pH
$\alpha\text{-}Fe_2O_3$	hematite
β	the full width at half maximum
$\gamma\text{-}Fe_2O_3$	maghemite
λ	the wavelength of the X-rays
θ	the diffraction angle

AOPs	advanced oxidation processes
ANOVA	analysis of variance
BET	Brunaur-Emmett Teller surface analysis
BOD	biological oxygen demand
CCD	central composite design
COD	chemical oxygen demand
DOE	Design of Expert
ESM	eggshell and eggshell membrane
FTIR	Fourier-transform infrared spectroscopy
ICP-OES	Inductively coupled plasma - optical emission spectrometry
RSM	response surface methodology
SEM-EDX	scanning electron microscopy coupled with energy dispersive X-ray
TGA	thermogravimetric analysis
UV-vis	ultraviolet-visible-infrared spectrophotometer
XRD	X-ray diffraction

LIST OF APPENDICES

CHAPTER 1

INTRODUCTION

1.1   Water Pollution in Malaysia

Water is important for human life. More than two thirds of Earth's surface is occupied by water; less than a third is taken up by land. Water resource quality has the potential to affect every facet of life. For instance, there would be no vegetation on land, no oxygen for animals to breathe and the planet would look entirely different than it does today. As Earth's population keeps growing, people are putting ever-increasing pressure on the planet's water resources. However, there are more wastes are being discharged to the water stream in conjunction to the development of various field of industrial technologies. In a sense, the quality of water is reduced and poorer water quality means water pollution (Laboy-Nieves, et al., 2008).

Water pollution usually being defined as one or more substances exist in the water to certain concentration that may cause problems for living organisms either humans, animals or plants. The main sources of the water pollutants are come from point sources or non-point sources. A point source is refer to a single source of pollution location such as discharging pipe from industries. Non-point source pollution is refer to different scattered sources instead of a single point. Nowadays, water pollution is a severe problem faced by most of the countries including Malaysia. The availability of water resources for human usage is significantly decrease due to the high treatment costs for contaminated water and the treated effluent is not readily to be used or consumed. Due to these reasons, it is difficult to ensure that there is sufficient amount of good quality to water supply to all consumer in Malaysia. (Ling, 2010).

Figure 1.1 shows that the river quality in Malaysia from 2005 to 2014. In year 2014, out of the 473 rivers monitored, 244 (52%) of the rivers are still clean, 186 (39%) were slightly contaminated and the other 43 (9%) were totally polluted. It was observed that the total number of clean river was dramatically decreased from 338 in 2005 to 244 in 2014. This represented that the water resources in Malaysia is being polluted.
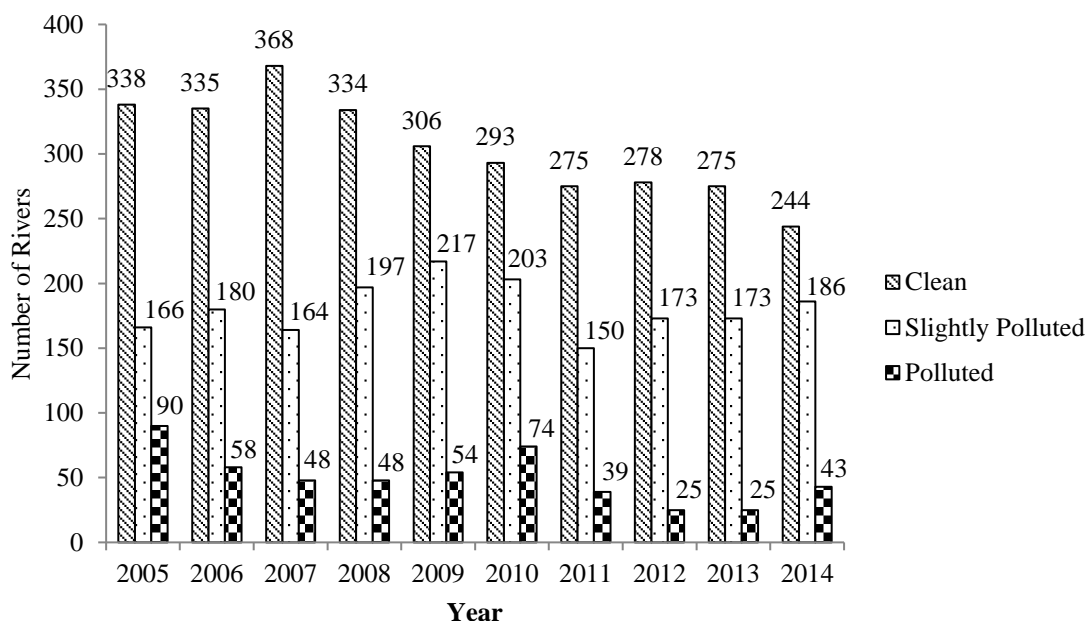
Figure 1.1: River Water Trend in Malaysia 2005-2014 (DOE, 2014)

1.2 Importance of Study

Dye is able to provide colour when you applied it to a substrate and give either a temporarily or permanent colour (Chequer, et al., 2013). It can be manufactured by two different ways which is either natural or synthetic. Natural dyes are extracted from plants, vegetables, fruit and flower but it cannot retain the colour for a long period. Therefore, synthetic dyes are used instead of natural dyes due to their high retaining properties throughout washing and exposure. Depending on the type of substance being dyed, many different types of dyes consist of various chemical compounds. For example, acid dyes are applied to animal fibre, basic dyes used for paper, direct dyes used for cotton-wool and pigment dyes used in paint and inks (Yusuf, Shabbir and Mohammad, 2017). Although the dyes are providing colour to our world, however, it will also bring a lot of negative impact to our environment. Dyeing industry has been considered as a great concern as it might bring adverse effect to our environment. Nowadays, over 10,000 different dyes and pigments are used in industry and over 7×10^5 tons of synthetic dyes are produced worldwide in a year (Chequer, et al., 2013). During dyeing process, it estimated that approximately 10-15% dyes are discharged into the water bodies with highly coloured and aesthetically unpleasant (Pandey, et al., 2018). There are more than 200,000 tons of these dyes are released to environment due to the improper dyeing process (Chequer, et al., 2013). The effluents from dyeing

industry are toxic, carcinogenic or mutagenic to living organisms. Therefore, the risk of getting disease is relatively higher near the polluted area than the area far from it.

Figure 1.2 indicates that China is the largest consumer of synthetic dye which account for 40-45% of world utilization. India expanded its quality and utilization up to 10% in the world. These two nations belong to the main exporters of dyes as compared to other countries.
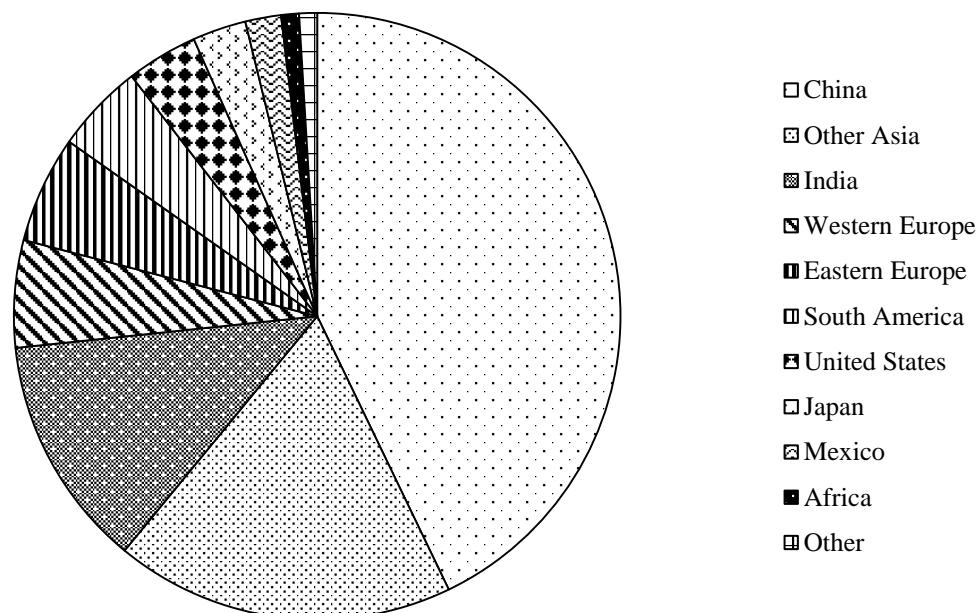
Figure 1.2: Global Dyes Market Demand (IHS, 2014)

The dye effluents are highly visible and undesirable because they are affecting aesthetic merit, transparency and gas solubility of water bodies (Pereira and Alves, 2012). For instance, it will reduce light penetration in river which may affect the photosynthesis of the flora and the food chain in aquatic life. The dissolved oxygen in water may be reduced due to the presence of thin layer of dyes that stay above the water surface, leading to insufficient oxygen supply to the organism in the river (Pereira and Alves, 2012). Therefore, the degradation of organic dyes is quite important to be explored and developed. Table 1.1 shows that the dye fixation on the textile product and percentage of dyes that loss to environment. It was shown that dyes were not completely fixed to the textile product and a certain amount of dyes being loss to the environment and finally cause water pollution issue.

Table 1.1: Fixation Degree of Various Dye Class (Joshi, Bansal and Purwar, 2004)

Dye Class	Fibre	Degree of Fixation %	Loss to Effluent %
Acid	Polyamide	80-95	5-20
Basic	Acrylic	95-100	0-5
Direct	Cellulose	70-95	5-30
Disperse	Polyester	90-100	0-10
Metal-Complex	Wool	90-98	2-10
Reactive	Cellulose	50-90	10-50
Sulphur	Cellulose	60-90	10-40
Vat	Cellulose	80-95	5-20

1.3   Problem Statement

From the environment impact of the dye discharged from dyeing industry, the decolourisation and degradation of the dye should be explored and developed. Since the rate of dye consumption and production of dye are increasing, more effective textile wastewater treatment should be conducted in order to track the amount of wastewater generated effectively. For instance, the decolourisation of the dye can be performed by physical, chemical and biological methods.

Physical treatments are absorption and ion exchange. Adsorption method to remove dyes could be attractive and effective method which depend on the type of the adsorbent used (Hmd, 2011). This technique is classified as non-destructive method since adsorption just transfer the pollutant from water to solid matrix. Meanwhile, coagulation is only capable to remove disperse dyes with high amount of sludge waste produced and may not effective to remove highly soluble dyes (Azbar, Yonar and Kestioglu, 2004). Biological treatment is a decolourisation method that degrade the textile dye by using microorganism. The major advantages of this treatment include simple operation and low cost treatment for huge volume of wastewater as compared to physical treatment. The utilised microorganism are biodegrade and bioadsorb the organic dyes from wastewater. However, the synthetic dyestuff with highly complex polyaromatic structure may not effective to be degraded by using biological method. The degree of degradation of the dye by using biological treatment can be determined by the biological oxygen demand (BOD) to chemical oxygen demand (COD). For

example, the dyes will be non-biodegradable if the ratio of BOD to COD is relatively low (Azbar, Yonar and Kestioglu, 2004).

Advanced oxidation processes (AOPs) are classified as chemical treatment for dye decolourisation. The objective of AOPs is to produce and utilise the hydroxyl free radicals ($\cdot$OH) to react with organic pollutants (Hmd, 2011). AOPs have a huge favourable circumstances over regular treatment techniques because no chemical or biological sludge being generated and able to achieve a total mineralisation of organic pollutants. This method has become a turning point in the textile wastewater field due to the high performance of AOP. Hydrogen peroxide (H_2O_2) reacts with ferrous ions is named as Fenton's reagent.

The generation of those radicals is accomplished by utilising either single oxidant or combination of O_3, H_2O_2 and UV radiation. Fenton process is one of the most promising AOPs because of high mineralisation achievement at mellow states of both temperature and pressure. Iron ions are used to catalyse the H_2O_2 to produce $\cdot$OH. One of the interesting point of the Fenton process is this process does not require high energy input and could be operated at ambient conditions. Furthermore, it requires short reaction time and utilising easily handle reagents. However, the primary disadvantage of homogeneous Fenton reagent catalyst is cannot be recovered from the effluent (Rossi, 2014). Therefore, the development and optimisation of heterogeneous Fenton process is essential in order to improve the effectiveness of the process.

The common catalyst used in heterogeneous Fenton process which usually is iron oxide. Iron oxide with suitable surface chemistry are manufactured by different methods such as wet chemical, dry processes, or microbiological techniques (Ali, et al., 2016). However, these methods will generate waste during manufacturing process and adversely affect the environment around us. Therefore, the synthesis of the iron oxide in a green way such as green approach using fruit peel extract as the biogenic reductant will be explored and developed.

1.4   Research Objectives

The main objective of this study is to synthesise the iron oxide catalyst used in Fenton process by using several types of fruit peels. There are several sub-objective are identified in order to achieve the main goal of this study:

1. To synthesise and characterise the iron oxide magnetic catalyst through a facile green approach using orange peels.

2. To optimise the operating parameters for heterogeneous photocatalytic, Fenton and Fenton-like reactions by using response surface methodology.

1.5   Scopes of Study

In this study, the synthesis of iron oxide catalyst is prior step for investigation of the degradation performance of this catalyst. The iron oxide catalyst is produced through the reduction of iron metal salts ($Fe(NO_3)_3 \cdot 9H_2O$) in the presence of several types of fruits peels extract. The synthesised iron oxide particles are immobilised on eggshell particles surface. The process behaviour of iron oxide particles with or without eggshell support has been studied.

Besides, the properties of iron oxide catalyst are determined by several test such as X-ray diffraction (XRD), scanning electron microscopy (SEM), Fourier-transform infrared spectroscopy (FTIR) and thermogravimetric analysis (TGA). XRD is a technique which used to study the crystal structure and morphology of the catalyst can obtained by SEM. FTIR is used for identification of functional group for inorganic and organic materials. TGA is conducted to determine the mass change of the sample as a function of time or temperature. In order to investigate the process behaviour of degradation, a series of experiment will be conducted to investigate various dye concentration, catalyst dosage and solution pH. Response surface methodology (RSM) is used to determine optimum condition of photocatalytic degradation of organic dyes.

CHAPTER 2

LITERATURE REVIEW

2.1   Classification of Dyes

Dyes are organic compounds which commonly used for colouring textile. They are different from paint which are absorbed into the pores of the material instead of develop on the fibre surface due to the size of the dye molecules is smaller than the size of the pores in the fibre. Since the different fibre materials and molecular structure of dyes, the application of dye on fibre material is mainly depends on the type of fibre material. There are different ways for classification of dyes either based on the source of materials or application.

The other classification method is based on the application such as which type of fibres can be applied. The dyes can be classified as acid dyes, basic dyes, direct dyes, disperse dyes, reactive dyes, sulphur dyes and vat dyes. Different types of dyes are applied to different materials or fibres with various degree of fixation. Table 2.1 indicates major dye classes, fixation rate and the types of fibres for fixation. The selection of dye depends on the types of fibres being dyed, desired shade, dyeing uniformity and fastness (Butler, et al., 2016). It is interesting to note that the percentage of dye fixation on fibre will never reach 100%. Therefore, some of the dye will be released to environment during dyeing process which may induce some environment impact. In order to reduce the dye effluent, the colour removal technique for textile effluents is quite important for this modern century.

Table 2.1: Classification of Textile Dye (Butler, at al., 2016)

Dye Class	Description	Method	Fibres Typically Applied to	Typical Fixation (%)	Typical Pollutants Associated with Various Dyes
Acid	Water-soluble anionic compounds	Exhaust/ continuous (carpet)	Wool, nylon	80-93	Colour; organic acids; unfixed dyes
Basic	Water-soluble, applied in weakly acidic dyebaths; very bright dyes	Exhaust	Acrylic, some polyesters	97-98	N/A
Direct	Water-soluble, anionic compounds; can be applied directly to cellulosic without mordants (or metals like chromium and copper)	Exhaust/ continuous	Cotton, rayon, other cellulosic	70-95	Colour; salt; unfixed dye; cationic fixing agents; surfactant; defoamer; levelling and retarding agents; finish; diluents

Disperse	Not water-soluble	High temperature exhaust/ continuous	Polyester, acetate, other synthetics	80-92	Colour; organic acids; carriers; levelling agents; phosphates; defoamers; lubricants;dispersants; delustrants; diluents
Reactive	Water-soluble, anionic compounds; largest dye class	Exhaust/ cold pad batch/ continuous	Cotton, other cellulosic, wool	60-90	Colour; salt; alkali; unfixed dye; surfactants; defoamer; diluents; finish
Sulphur	Organic compounds containing sulphur or sodium sulphide	Continuous	Cotton, other cellulosic	60-70	Colour; alkali; oxidising agent; reducing agent; unfixed dye
Vat	Oldest dyes; more chemically complex; water-insoluble	Exhaust/ package/ continuous	Cotton	80-95	Colour; alkali; oxidising agents; reducing agents

2.2   Colour Removal from Textile Effluent

Physical treatments involve any process which does not contribute chemical reaction or biological changes (Muralikrishna and Manickam, 2017). There are several physical methods such as sedimentation and membrane separation. Sedimentation is a process conducted by the effect of gravity, the particles in the suspension are allowed to settle down and removed later. Sedimentation usually is applied for the pre-treatment process for coagulation to reduce chemical used for coagulation (Gregory and Edzwald, 2010).

Membrane separation is one of the separation technologies that used for colour removal from textile effluent. The wastewater are flowing through a selective film and separation occurred by restricting the particle size larger than the pore on the film (Si, et al., 2013). Nanofiltration, ultrafiltration and reverse osmosis are considered as membrane separation (Arafat, 2007). Table 2.2 shows that the filtration scope for different types of membranes. For colour removal from textile effluent, suitable membrane for decolourization are nanofiltration and reverse osmosis due to smaller membrane pore size than dye molecules. However, the major problem which related with these techniques are membrane fouling caused by precipitation of several materials such as calcium, silica, barium, strontilim and iron. This condition may lead to bacteria preliferate in the membrane (Upadhye and Joshi, 2012).

Adsorption is an alternative method for colour removal from textile wastewater which involve liquid-solid interface. Despite the pollutants transferred from liquid phase to solid phase, adsorption process is considered an effective method for wastewater treatment due to its capable in capture and entrapment of materials with extremely small size of adsorbent (Körlüa, et al., 2015). During adsorption, the pollutant molecules in the liquid phase are attached to the solid surface which driving by the attractive force on the solid surface. The efficiency of the adsorption is mainly depends on the types of the adsorbent. The most common type of adsorbent is activated carbon. Although adsorption processes are able to produce high quality of water, the adsorbent materials are sometimes expensive and hard to be reactivated (Saqib Nawaz and Ahsan, 2014).

Table 2.2: Filtration Scope of Different Membrane (Upadhye and Joshi, 2012)

Process	Pore Size (Micro)	Molecular Weight (g/mol)	Examples
Microfiltration	0.001-2.0	>100000	Bacteria
Ultrafiltration	0.002-0.1	1000-200000	Colloids, virus, protein, etc.
Nanofiltration	0.001-0.07	180-15000	Dyes, pesticides, divalent ions, etc
Reverse Osmosis	<0.001	<200	Salts & ions

Ion exchange processes are widely used as purification, separation and decontamination of aqueous or ion containing solution (Kansara, et al., 2016). Ion exchange processes are able to remove one or more contaminants from water through exchange with another non-objectionable or less objectionable materials. It can be classified on the positive or negative ion exchange such as cation exchanger or anion exchanger (Mohammad, et al., 2017). Ion exchange resin usually operated based on a cyclic basis. First of all, the water is flow through the basis until it becomes saturated and followed by regeneration through backwashing the resin to remove the accumulated solids (Kansara, et al., 2016). However, ion exchange processes are not widely used for treatment of textile effluent due to the resins usually are not effective to treat a wide range of dyes especially disperse dyes and the cost for regeneration is quite expensive (Joshi, Bansal and Purwar, 2004).

Coagulation and flocculation processes are belong to physico-chemical treatment which can be used to remove the dyes with high molecular weight. Coagulation and flocculation processes do not involve partially or fully decomposition of dyes (Mane and Babu, 2011). The most common coagulants used for textile wastewater treatment are alum, ferrous sulphate and magnesium chloride in combination with lime. The function of coagulants is to convert the colloidal and dispersal particles into smaller flocs which reduce the magnitude of the repulsive interactions between particles and destabilisation of the particles. In flocculation process, the particles are produced by means of aggregation which can be removed by simple separation processes such as gravity sedimentation and filtration (Solanki, et al., 2013). Although the physio-chemical treatment can be effective in dye removal, a

certain amount of physico-chemical sludge will be formed and proper disposal is required (Saqib Nawaz and Ahsan, 2014).

Biological wastewater treatment utilised microorganisms such as bacteria, protozoa in tanks under either anaerobic or aerobic process. Normally, biological wastewater treatment is treated as secondary treatment. Sufficient oxygen and food are supplied to microorganism in order to maintain their activities (Samer, 2015). Aerobic treatment such as aeration lagoon are normally take place in the presence of air, aerobes to convert organic impurities into carbon dioxide, water and biomass (Subashini, 2015). Meanwhile, anaerobic treatment such as anaerobic digestor and anaerobes which do not require air to assimilate organic pollutant to generate methane, carbon dioxide and biogas (Subashini, 2015). Although biological treatment becomes integral part of many wastewater treatment plant, but it still not effective in degradation of some synthetic dyestuffs due to the complicated polyaromatic structure and recalcitrant nature of dyes (Azbar, Yonar and Kestioglu, 2004). Besides, there are several drawbacks of biological treatment such as aerobic digestion generates substantial amount of biogas which may cause overgrowth or eutrophication, while anaerobic processes are quite less efficient than aerobic processes with a smaller range of contaminants bring attacking.

One example of chemical wastewater treatment is chlorination. Chlorine was effectively utilised for wastewater treatment. In textile industry, chlorination will decolourises wastewater by oxidation when pure chlorine is added to water. After that, the chlorine will quickly breakdown into hypochlorous acid (HOCl) followed by dissociates into hypochlorite ions (OCl$^-$). HOCl and OCl$^-$ are strong oxidising agents which are able to degrade the dyes in the wastewater (Barnhert, Allen, and Barnhart, 1993). The main drawback of chlorination is high cost of the chlorine which will increase the overall cost of wastewater treatment (Quader, 2010). Besides, dechlorination process should be conducted in order to prevent the toxic effect in biological processes. Similar to ion exchange process, chlorination process is not effective to treat a wide range of dyes especially direct and disperse dyes (Joshi, Bansal and Purwar, 2004).

2.3   Advanced Oxidation Processes

AOPs are alternative method to degrade the organic contamination effectively. AOPs consist of several powerful technologies such as ultra-violet, O_3, H_2O_2 and oxygen. The strong oxidising agents are able to degrade recalcitrant organic pollutants and inorganic pollutants (Deng and Zhao, 2015). Chemical oxidation processes such as Fenton process, ozonation, photocatalytic degradation and electrochemical oxidation are considered as AOPs (Ribeiro, et al., 2015). AOPs able to produce adequate amount of high powerful non-selective ·OH in order to oxidise most of the organic pollutants in the wastewater (Hassaan, ElNemr and Madkour, 2017). Conventional AOPs can be also divided into homogeneous and heterogeneous processes depend on the phase of catalyst used. (Ribeiro, et al., 2015).

Table 2.3 shows the standard oxidation potential for different oxidants and the oxidation potential of ·OH is relatively higher than the others, thus it is sufficient for degradation of various recalcitrant organic pollutants (Babuponnusami and Muthukumar, 2014). Figure 2.1 shows Fenton process is the mostly applied AOPs which approximately 31% on overall basis and followed by heterogeneous photocatalysis which consist of 20% (Ribeiro, et al., 2015).

Table 2.3: Standard Oxidation Potential of Common Oxidants (Babuponnusami and Muthukumar, 2014)

Oxidant	Oxidation potential (V)
Fluorine (F_2)	3.03
Hydroxyl Radial (·OH)	2.80
Atomic Oxygen (O)	2.42
Ozone (O_3)	2.07
Hydrogen Peroxide (H_2O_2)	1.77
Potassium Permanganate ($KMnO_4$)	1.67
Chlorine Dioxide (ClO_2)	1.50
Hypochlorous Acid (HClO)	1.49
Chlorine (Cl_2)	1.36
Oxygen (O_2)	1.23
Bromine (Br_2)	1.09
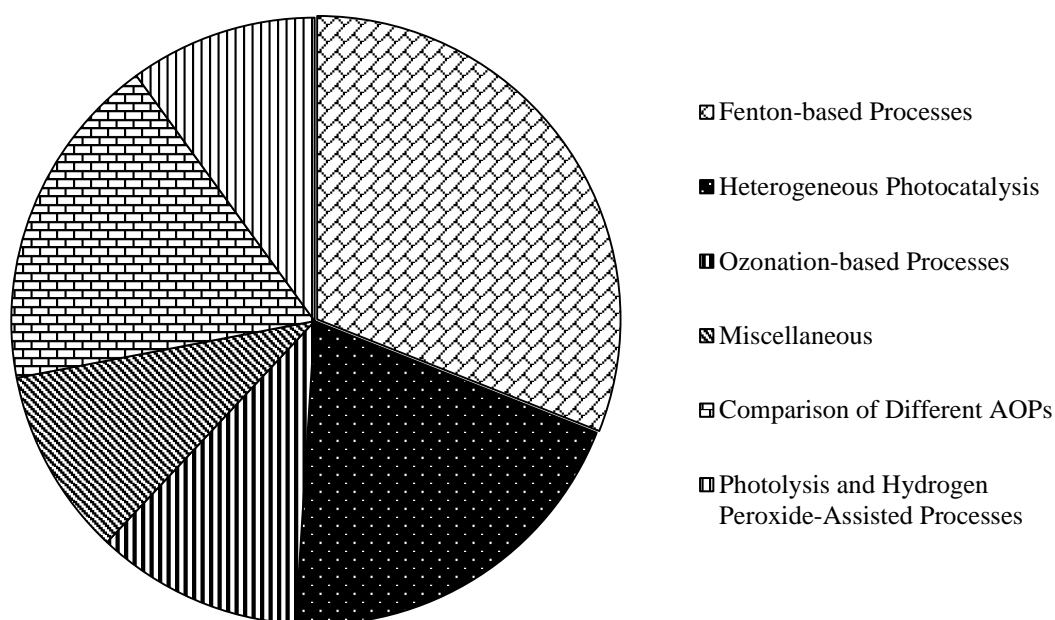
Figure 2.1: Different Types of AOPs (Ribeiro, et al., 2015)

2.3.1 Fenton and Fenton-like Processes

Fenton process is one of the most important AOPs which widely used in textile wastewater treatment. It involves the reactions of H_2O_2 with iron ions under acidic condition to generate active oxygen species which are able to degrade organic or inorganic pollutants (Sreeja and Sosamony, 2016). The Fenton process was first discovered in 1894 by Henry John Horstman Fenton, who discovered that H_2O_2 could react with ferrous ions to oxidise tartaric acid (Fenton, 1894). It can further classified into homogeneous and heterogeneous. In homogeneous condition, ferrous ions are normally used as fenton reagent to produce ·OH and perhydroxyl radicals (·O_2H) from water molecule. Meanwhile, in heterogeneous conditions, iron catalysts are immobilised on a support such as chitosan (Fontecha-Cámara, et al., 2011).

The mechanisms of Fenton process are shown by equations (2.1) to (2.5) (Babuponnusami and Muthukumar, 2014). Equation (2.1) represents the oxidation of ferrous ions (Fe^{2+}) to ferric ions (Fe^{3+}) to decompose H_2O_2 into ·OH. The generated ferric ions are involve in the reaction (2.2) with excess H_2O_2 to produce Fe^{2+} and ·O_2H. This reaction is called Fenton-like reaction which consist of a looping relationship with Fenton reaction. However, Fenton-like reaction rate is much slower than Fenton reaction and lead to a cyclic mechanism from Fe^3 to Fe^{2+}. The species produced in the

Fenton-like reaction is $\cdot O_2H$ instead of $\cdot OH$ with lower reactivity compared to $\cdot OH$. Last but not least, equation (2.6) shows the radical-radical reaction occur in Fenton process to utilise excess amount of $\cdot OH$ to form H_2O_2.

$$Fe^{2+} + H_2O_2 \rightarrow Fe^{3+} + OH^- + \cdot OH \qquad (2.1)$$

$$Fe^{3+} + H_2O_2 \rightarrow Fe^{2+} + \cdot O_2H + H^+ \qquad (2.2)$$

$$Fe^{2+} + \cdot OH \rightarrow Fe^{3+} + OH^- \qquad (2.3)$$

$$Fe^{3+} + \cdot O_2H \rightarrow Fe^{3+} + HO_2^- \qquad (2.4)$$

$$Fe^{3+} + \cdot O_2H \rightarrow Fe^{2+} + O_2 + H^2 \qquad (2.5)$$

$$\cdot OH + \cdot OH \rightarrow H_2O_2 \qquad (2.6)$$
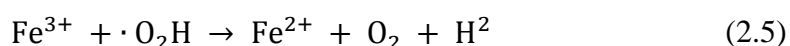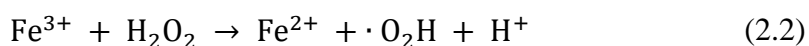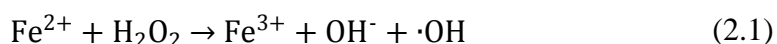
The main advantage of Fenton process can be carried out at room temperature and does not require high energy supply. In addition, the Fenton reagents are easy to obtain, store and handle safely which do not induce environmental damages (Pignatello, Oliveros and MacKay, 2006). Although Fenton process has provide high dye degradation, there are several drawbacks need to be resolved such as unattainable regeneration of catalyst and narrow pH operating range. Huge amount of iron sludge generated may not only cause secondary pollution but also restrain the reliability of Fenton process in wastewater treatment. Therefore, the removal of iron sludge is quite important, as it will lead to the overall process becomes complicated and uneconomical (Guo, et al., 2017).

The pH value plays a decisive role in the oxidation potential of $\cdot OH$ radicals due to the reciprocal relationship of the oxidation potential to the pH value. Adityosulindro (2017) stated that the efficiency of Fenton reaction was reduced at extreme pH value. For instance, the oxidation potential of $\cdot OH$ reduce at high pH value condition due to the decomposition of H_2O_2 into ^-O_2H, water (H_2O) and oxygen (O_2) (Adityosulindro, 2017). In additions, low efficiency of Fenton reaction at high pH can also be explained by the generation of relatively inactive iron oxohydroxides and ferric hydroxide precipitate which may reduce the amount of $\cdot OH$ generated in the presence of limited free iron ions (Babuponnusami and Muthukumar, 2014). Besides, iron active species will tend to convert into iron complexes at low pH condition which provide slow response with H_2O_2. Furthermore, $\cdot OH$ can be scavenged by H^+, while H_2O_2 can be stabilised through the formation of oxonimum ion ($H_3O_2^+$) which tend to reduce the

reactivity with ferrous species and lead to low process efficiency (Adityosulindro, 2017). Deng and Zhao (2015) concluded that the homogeneous Fenton process was only effective at an acidic pH condition which typically around from 3.0 to 4.0. In a nutshell, narrow operating pH condition will obviously increase the treatment cost and difficulties in the storage, transportation and handling of acid condition (Deng and Zhao, 2015).

The operating conditions of Fenton reactions are playing important role to desirable results. In addition, the separation of catalyst from the treated water is important. Through the consideration of these factors, the application of heterogeneous Fenton process is possible to improve the ·OH production and reduce the amount of ferric sludge (Hassani, et al., 2018). Heterogeneous Fenton process utilises the heterogeneous catalyst which may overcome some of the drawbacks for classic homogeneous Fenton reaction. There are several types of catalysts that can be used as Fenton oxidation catalyst such as iron oxide minerals (*e.g.* magnetite, pyrite) and iron oxide immobilised on high specific area materials (*e.g.* activated carbon, alumina) (Adityosulindro, 2017).

Adityosulindro (2017) stated that there were two possible mechanisms for the heterogeneous Fenton reaction. For the first mechanism, iron surface species on the catalyst is directly induce a heterogeneous Fenton reaction mechanism. On the other hand, the iron species are easily leached in solution which tend to induce a homogeneous Fenton reaction. Equation (2.7) indicates that the reaction of Fe^{2+} and H_2O_2 if Fe^{2+} exists on the catalyst surface. Equations (2.8) and (2.9) shows a complex is formed by the reaction of Fe^{3+} which located on catalyst surface with H_2O_2, followed by converted into Fe^{2+}. Another mechanism was proposed by Fang, Zhou and Dionysiou (2013) which respect to the generation of ·OH by magnetite (Fe_3O_4) as present in equations (2.10) to (2.15). First, a series of single electron transfer reactions will lead the Fe^{2+} dissolved from Fe_3O_4 react with O_2 to produce $O_2^{\cdot-}$. This followed by $O_2\cdot-$ react with Fe^{2+} through second single electron transfer to produce O_2^{2-} and rapidly protonated to form H_2O_2. Finally, the ·OH is produced by another single electron transfer from H_2O_2. Figure 2.2 indicates the mechanism pathway of ·OH generating by Fe_3O_4 which proposed by Fang, Zhou and Dionysiou (2013).

$$Fe^{2+}_{surface} + H_2O_2 \rightarrow Fe^{3+}_{surface} + OH^- + \cdot OH \qquad (2.7)$$

$$\text{Fe}^{3+}_{\text{surface}} + \text{H}_2\text{O}_2 \rightarrow \text{Fe}^{3+}_{\text{surface}}(\text{H}_2\text{O}_2) \tag{2.8}$$

$$\text{Fe}^{3+}_{\text{surface}}(\text{H}_2\text{O}_2) \rightarrow \text{Fe}^{2+}_{\text{surface}} + \cdot\text{OOH}(\cdot\text{O}_2^-) + \text{H}^+(2\,\text{H}^+) \tag{2.9}$$

$$\text{Fe}^{2+} + \text{O}_2 \rightarrow \text{Fe}^{3+} + \cdot\text{O}_2^- \tag{2.10}$$

$$\text{Fe}^{2+} + \cdot\text{O}_2^- + 2\text{H}^+ \rightarrow \text{Fe}^{3+} + \text{H}_2\text{O}_2 \tag{2.11}$$

$$\cdot\text{O}_2^- + \text{H}^+ \rightarrow \cdot\text{O}_2\text{H} \tag{2.12}$$

$$2\cdot\text{O}_2^- + 2\text{H}^+ \rightarrow \text{H}_2\text{O}_2 + \text{O}_2 \tag{2.13}$$

$$\text{Fe}^{2+} + \text{H}_2\text{O}_2 \rightarrow \text{Fe}^{3+} + \text{OH}^- + \cdot\text{OH} \tag{2.14}$$

$$\cdot\text{O}_2^- + \text{H}_2\text{O}_2 + \text{H}^+ \rightarrow \text{O}_2 + \text{OH}^- + \text{H}_2\text{O} \tag{2.15}$$
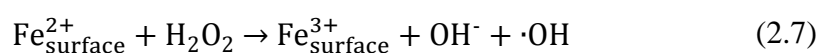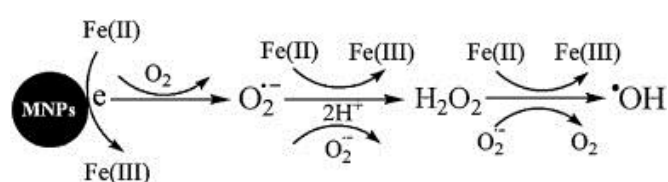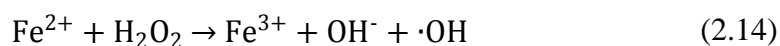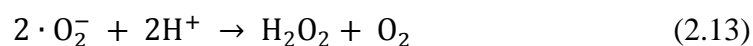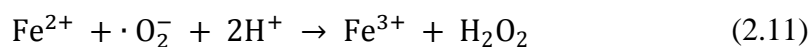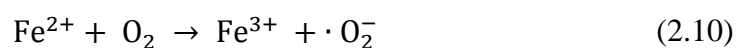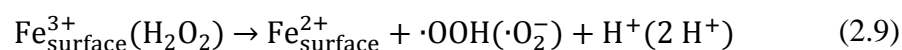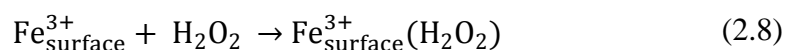
Figure 2.2: The Mechanism of ·OH Generation by Fe$_3$O$_4$ (Fang, Zhou and Dionysiou, 2013)

In heterogeneous Fenton process, the chemical reactions are only take place on the active sites above on the catalyst surface. After completion of reactions, the product molecules are finally desorbed and leave from the active sites which followed by a new set of reactant molecules are attached to the surface and repeated the process. Thus, heterogeneous process possess several benefits such as less iron sludge production and easy separation between the catalyst and solution (Sreeja and Sosamony, 2016). Xavier, et al. (2015) reported that high degree of decolourisation of dye in the case of the heterogeneous Fenton system could achieve in pH range from 2 to 7. It was found that the heterogeneous Fenton process was quite suitable at lower pH of 2. This was due to the formation of more oxidants at lower pH and also the adsorption between the negatively charged and positively charge of catalyst surface at low pH condition could be improved. Although the efficiency of both processes are reduced as increasing the solution pH, heterogeneous Fenton process will offer a wide range of solution pH as compared to homogeneous pathway (Xavier, et al., 2015). Table 2.4 concludes the difference between homogeneous and heterogeneous Fenton process in several properties.

Table 2.4: Different Properties of Homogeneous and Heterogeneous Fenton Process

Properties	Homogeneous Process	Heterogeneous Process
Phase	Single phase	More than one phase
pH	Narrow pH range	Wide pH range
	Optimum pH: 2.5-3.5	Optimum pH: 2-7
Sludge production	Iron sludge produced	Less iron sludge produced
Catalyst recovery	Complicated and uneconomical	Easy separation

2.3.2 Photocatalytic Reaction

Heterogeneous photocatalysis is conducted by using semiconductors such as titanium dioxide (TiO_2) or iron oxide which allow a complete mineralization for great variety of organic pollutants (Rajamanickam and Shanthi, 2016). This process is able to degrade water pollutants such as various types of organic dyes or complex mixture of water contaminants into carbon dioxide, water, and mineral acid (Xu, Rangaiah and Zhao, 2014).

The mechanism of photocatalysis reactions are shown by equations (2.16) to (2.19). When sufficient energy that is equal to or higher than band gap energy of UV-irradiated semiconductors, UV-irradiated with hole and electron hole pairs are produced as shown in equation (2.16). Equations (2.17) to (2.19) indicate the reactions occur at the surface of catalyst to further produce $\cdot OH$ from OH^-, H_2O and O_2 (Deng and Zhao, 2015). In addition, $\cdot OH$ can be produced by the reaction of holes with H_2O or OH^- which adsorbed on the surface of semiconductor (Abdennouri, et al., 2016). Table 2.5 shows some advantages and limitation of heterogeneous photocatalysis.

$$TiO_2 + hv \ \rightarrow \ e_{cb}^- + hv_{vb}^+ \tag{2.16}$$

$$hv_{vb}^+ + \ OH_{surface}^- \rightarrow OH \cdot \tag{2.17}$$

$$hv_{vb}^+ + \ H_2O_{absorbed} \ \rightarrow \ OH \cdot \ + H^+ \tag{2.18}$$

$$e_{cb}^- + \ O_{2 \ absorbed} \ \rightarrow \ O_2^{\cdot -} \tag{2.19}$$

$$hv_{vb}^+ + \text{Pollutant}_{ads} \ \rightarrow \cdot \text{Pollutant}_{ads}^+ \ \rightarrow \text{Degradation Products} \tag{2.20}$$
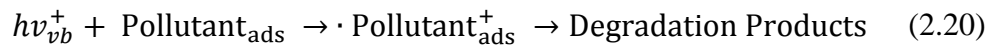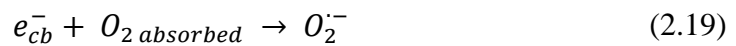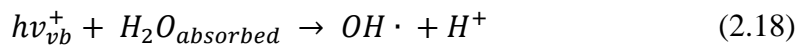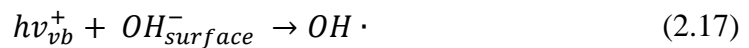
Table 2.5: Advantages and Limitations of the Photocatalytic Reaction (Saravanan, Gracia and Stephen, 2017)

Advantages	Limitations
Good replacement for the energy-intensive conventional treatment methods.	Interfacial charge transfer.
Lead to formation of harmless products.	Improve the charge separation.
Destruction of a variety of hazardous compounds.	Inhibition of charge carrier recombination.
Reaction conditions are mild and reaction time is modest.	
Minimal generation of secondary waste.	
Hydrogen generation, gaseous phase and aqueous treatments can be applied.	

Photocatalytic degradation techniques have receive a great attention in the field of wastewater treatment because the complete mineralization can be achieved at mild operating temperature and pressure. TiO_2 is the most common used photocatalyst due to its high photo-activity, high chemical and thermal stability, low toxicity and relatively lower cost. Besides from TiO_2, Fe_2O_3 can also be a good semiconductor for photocatalysis reaction due to strong oxidation power from its valence band edge that exceeding the standard redox potential of H_2O and O_2 (Giannakis, et al., 2017). The mechanism of photocatalytic degradation in the presence of iron oxide is shown in Figure 2.3. Other advantages for using Fe_2O_3 include high purity can be obtained easily, long wavelength absorption properties and high irradiation stability.

The mechanisms of photocatalytic reaction by Fe_2O_3 is similar to the presence of TiO_2 which have been shown as equations (2.16) to (2.20). Apart from photocatalytic reaction to produce reactive oxidation species (ROSs), the Fe^{2+} and Fe^{3+} are easily leached from the surface of Fe_2O_3 which should be consider for radical generation (Fang, Zhou and Dionysiou, 2013). The equation (2.21) shows the H_2O_2 will be produced by the reaction of e^-, $O_2\cdot^-$ and $2H^+$ as proposed by Giannakis, et al. (2017). There are major advantages of Fe_2O_3 used as photocatalyst, the treatment not only carried by photocatalytic mechanism but also Fenton and Fenton-like reaction mechanism and lead to the high amount of ROSs.

$$e_{cb}^- + O_2^{\cdot-} + 2H^+ \rightarrow H_2O_2 \tag{2.21}$$
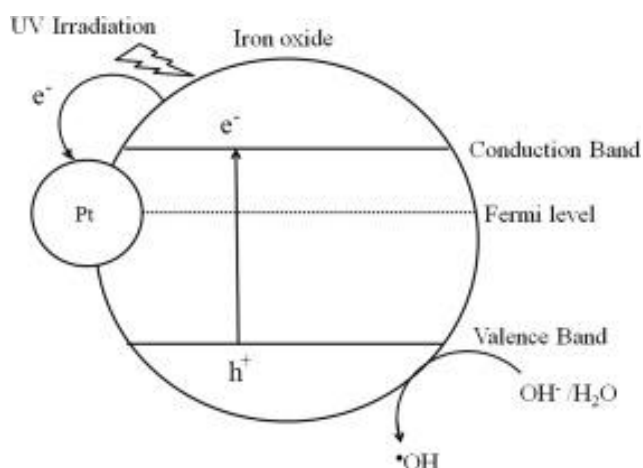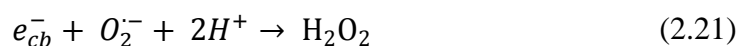
Figure 2.3: Photocatalytic Reaction by Iron Oxide (Liang, et al., 2014)

2.4 Iron Oxide

Iron oxide is commonly exist in the nature with various structures such as Fe_3O_4, maghemite (γ-Fe_2O_3) and hematite (α-Fe_2O_3). In the past, the researches about the synthesis and application of iron oxide with relatively new properties and functions are highly interesting. In addition, it is possible to provide high functioning to various field due to several reasons such as easy synthesis, coating or modification and manipulation of matter on an atomic scale. Furthermore, iron oxide nanomaterials play important role in biotechnology field due to their low toxicity, chemical inertness and biocompatibility (Xu, et al., 2012). Pang, et al. (2015) proposed that the good photocatalytic performance can be achieved by using Fe_3O_4, γ-Fe_2O_3 and α-Fe_2O_3 as photocatalyst due to their appropriate valence band position for oxygen evolution and narrow band gap energies which support in generating electron-hole pairs to perform reduction and oxidation processes. Teja and Koh (2009) concluded the properties of different form of iron oxide in Table 2.6.

Iron oxide is abundant in earth crust which consists of more than one crystal structure with different structural and magnetic properties. The crystal structure of the iron oxide can be classified as the interstitial sites of close packed planes of oxygen anions and iron cations at octahedral or tetrahedral respectively (Campos, et al., 2015). α-Fe_2O_3 is a type of iron oxide which was first discovered and obtained easily in earth crust such as rocks and soils. Different colours can be observed from α-Fe_2O_3 depend

on finely divided or coarsely crystallite. Fine α-Fe_2O_3 will appear blood-red and coarse α-Fe_2O_3 will appear black or grey (Teja and Koh, 2009). Guo, et al. (2010) stated that α-Fe_2O_3 is more chemically and thermally stable than other iron oxide crystallite polymorphs (Guo, et al., 2010). Fe_3O_4, as formula $Fe^{3+}(Fe^{2+}, Fe^{3+})O_4$ which presents highly magnetization condition under normal condition but the chemical stability is relatively low due to the ability to dissolve in acidic medium easily (Pang, et al., 2015). γ-Fe_2O_3 occurs as a weathering product of Fe_3O_4te in the soil or as a heating product of other iron oxides. It is thermally unstable and easily form α-Fe_2O_3 at higher temperature (Campos, et al., 2015).

Table 2.6: The Properties of Different Iron Oxides (Teja and Koh, 2009)

Property	Hematite	Magnetite	Maghemite
Molecular formula	α-Fe_2O_3	Fe_3O_4	γ-Fe_2O_3
Density (g/cm³)	5.26	5.18	4.87
Melting point (ºC)	1350	1583-1597	-
Hardness	6.5	5.5	5
Type of magnetism	Weakly ferromagnetic or antiferromagnetic	Ferromagnetic	Ferrimagnetic
Crystallographic system	Rehombohedral, hexagonal	Cubic	Cubic or tetrahedral
Stuctural type	Corundum	Inverse spinel	Defect spinel

The classification of crystal structure of iron oxide depends on the position of iron cations in close packed planes of oxygen anions, either octahedral or tetrahedral interstitial sites (Campos, et al., 2015). The corundum and rhombohedral structure of α-Fe_2O_3 which comprised of an ion O^{2-} reticle as a close-packed hexagonal crystallographic system and approximately two-thirds of the octahedral interstices in alternate layers are occupied by Fe^{3+} ions (Teja and Koh, 2009). The spinel crystal structure of γ-Fe_2O is similar to Fe_3O_4 where the oxygen ions are located in a cubic close-packed arrangement. Differ from Fe_3O_4, the vacancies in cation sublattice are about two-third of the sites which occupied by Fe^{3+} ions in regular arrangement with two filled sites being followed by one vacant site (Campos, et al., 2015). Among other

iron oxide, Fe_3O_4 consists of both bivalent and trivalent iron which Fe^{3+} distributed randomly between octahedral and tetrahedral sites and Fe^{2+} can be found in octahedral sites (Wu, et al., 2015). Figure 2.3 shows that the crystal structure of three different crystallite iron oxide (Wu, et al., 2015).
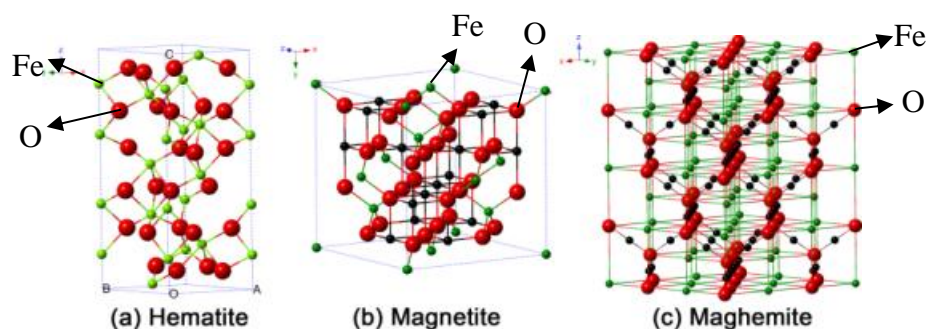
Figure 2.4: Crystal Structure of Hematite, Magnetite and Maghemite (Wu, et al., 2015)

The photocatalytic performance is mainly depends on the ability of adsorption, amount of electron-hole pair generation and the separation of the electron-hole pair. Wu, et al. (2015) discovered that α-Fe_2O_3 would provide relatively high photocatalytic activity for degradation of pollutant such as toluene as compared with γ-Fe_2O_3 and Fe_3O_4. First of all, the alternative parallel arrangement of Fe^{3+} and O^{2-} ions to the {0 0 1} plane in α-Fe_2O_3 lead to high surface energy and more progressive in photocatalysis than other faces. Besides, the relative narrow band gap (2.2 eV) of α-Fe_2O_3 will benefits in the longer photo-response to visible light region and improve the formation of electron-hole pair. The recombination rate occurred by α-Fe_2O_3 are relatively low due to high reactive {0 0 1} and {1 1 0} planes favour high separation efficiency. For γ-Fe_2O_3 and Fe_3O_4, the relatively low photocatalysis efficiency might be due to the low reactive {1 -1 -1} and {-1 1 2} which exposed exclusively (Wu, et al., 2015). Due to the above reasons, it could be concluded that α-Fe_2O_3 would provide more tremendous potential in photocatalytic degradation.

2.4.1 Synthesis Method of Iron Oxide

Up to now, there are several methods had been developed to synthesise iron oxide which can be classified to physical, chemical and biological methods. Chemical methods are widely used and developed as compared to physical and biological

methods such as co-precipitation, thermal decomposition, and hydrothermal synthesis (Ali, et al, 2016). Among these methods, co-precipitation is the most conventional method for synthesis of iron oxide because of high yield can be achieved by low production cost. In this method, iron oxide are synthesised by mixing Fe^{2+} and Fe^{3+} in a certain molar ratio under highly basic condition at room temperature or high temperature (Wu, He, and Jiang, 2008). There are several parameters that affect size and shape of iron oxide such as the type of metal salt used, the ratio between Fe^{2+} and Fe^{3+}, operating temperature, operating pH value and the ionic strength of the media (Ali, et al, 2016). However, this method is limited by certain drawbacks such as utilise harmful chemical, discharge deadly residue and lead to the contamination of environment (Rajiv, et al., 2017).

Therefore, an environmental friendly and biocompatible synthesis method is required to avoid some undesired ecological and negative impacts. Recently, green synthesis method had been explored and identified that it is an environmental friendly and low production cost approach (Al-Ruqeishi, Mohiuddin and Al-Saadi, 2016). For instance, one of the most widely used alternative techniques is utilising the plant extracts as reductant to synthesis metal oxide from metal salt solution. Simple, low production cost and environmental friendly approach are the main features that lead to this method a real alternative to the conventional method. In this method, plant extracts contribute a dual role in the synthesis which reduce the iron salt solution to iron oxide and acts as stabiliser to reduce the aggregation of the synthesised iron oxide. In addition, immobilising the iron oxide on the porous support is a good way to reduce operational problem and enhance the reusability (Martínez-Cabanas, et al., 2016).

2.4.2   Characterisation of Iron Oxide

Characterisation plays an important role in the development of nanoparticles. Characteristics such as the identification of the structures, composition, and chemical properties of nanoparticles are important factors to comprehend the relationship between the properties and its performance. In the development of more active, selective and durable catalyst or optimization of reaction conditions, this characterisation knowledge will becomes crucial (Zaera and Ma, 2006). In this case, several techniques are utilised to determine the physical and chemical properties of catalyst such as XRD, SEM, FT-IR and TGA.

XRD is a powerful non-destructive technique which commonly used to determine the bulk structure of crystalline materials. In addition, it able to provide information other than structure such as phases, crystal orientation, average grain size, crystallinity, crystal defect and strain (Bunaciu, Udriştioiu and Aboul-Enein, 2015). XRD technique operates to produce peaks through constructive interference of a monochromatic beam of X-rays scattered from every lattice planes with certain angle in a sample. This unique XRD peak pattern related with individual solid to determine the bulk crystalline components in the solid (Zaera and Ma, 2006). Thus, XRD pattern can be considered as the fingerprint of a certain material.

The basic principle of XRD is the interaction of the incident X-rays with crystalline sample to produce constructive interference and diffracted ray which obey Bragg's law (Bunaciu, Udriştioiu and Aboul-Enein, 2015):

$$n\lambda = 2dsin\theta \tag{2.22}$$

where

n = integer

λ = the wavelength of the X-rays

d = the interplanar spacing generating the diffraction

θ = the diffraction angle

In this technique, X-rays are produced by cathode ray tube and approach to monochromatic properties through filtration of the X-rays. Consequently, the incident ray will irradiate to the sample after focusing. The random orientation of the crystalline solid will lead to several possible diffraction directions of the lattice through a range of 2θ angles. Through the transformation of diffraction peaks to d-spacing, the determination of compound can be done due to unique d-spacing corresponding to specific compound (Bunaciu, Udriştioiu and Aboul-Enein, 2015).

Not only that, X-rays diffraction can also utilised to determine the average particle size of the sample. For instance, the sample with sufficient longer order, its peaks will present more intense and sharp, while its peaks become broader when particle size below about 100 nm. The Scherer's equation (2.23) can be used to estimate the crystalline size (D_c) of the sample (Lassoued, et al., 2017).

$$D_c = \frac{K\lambda}{\beta cos\theta} \qquad (2.23)$$

where

K = shape factor, 0.9

λ = the wavelength of the X-rays, (0.15148nm for CuK$_\alpha$)

β = the full width at half maximum

θ = the diffraction angle

There are six characteristic peaks can be observed with $2\theta = 30.3^\circ$, 35.6°, 43.2°, 53.5°, 57.2° and 62.9° for iron oxide. These peak are attributed to their corresponding indices {220}, {311}, {440}, {422}, {511} and {440} which the spinel structure of iron oxide such as Fe_3O_4 and γ-Fe_2O_3 can be identified (Gruskiene, et al., 2018). Besides, pure α-Fe_2O_3 can be identified by characteristic peak appearing at $2\theta = 24.16^\circ$, 33.12°, 35.63°, 40.64°, 49.47°, 54.08° and 57.42° associated to their corresponding indices {012}, {104}, {110}, {113}, {024}, {116} and {0.18} (Lassoued, et al., 2017).

The scanning electron microscopy (SEM) is a standout amongst the most generally utilised instruments in material research facilities. Several information can be provided by SEM which associated to topography and morphology (Leonard, Chandler and Seraphin, 2012). In microscope, the electron can be emitted from different sources and accelerated through an evacuated column by positive electrical potential. The electrons produced along this way is called primary electron. It can filter out any unscattered electron to generate a finely focused electron beam and subject to the surface of specimen. Consequently, several interactions will occur and produce various charged particles and photons such as backscattered electrons and secondary electrons as electron signals. Those emitted electrons from the specimen can be collected and used to form an image. Figure 2.6 indicates the SEM images of α-Fe_2O_3, γ-Fe_2O_3 and Fe_3O_4 in spherical shape (Prodan, et al., 2013; Gopal, et al., 2015; Lassoued, et al., 2017).
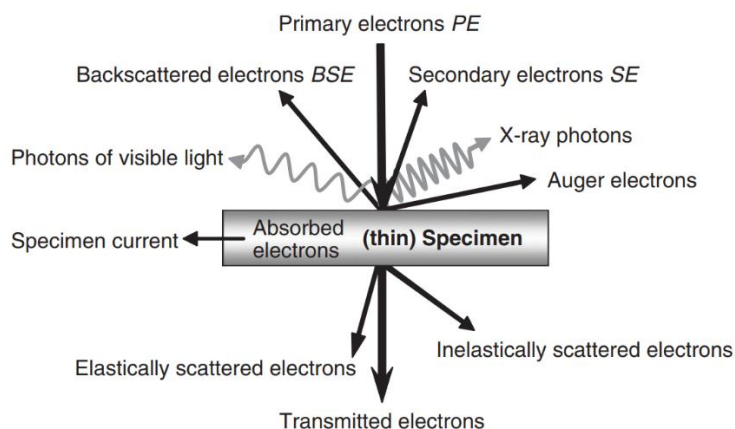
Figure 2.5: The Electron Generation of Useful Signal on the Specimen (Stokes, 2008)
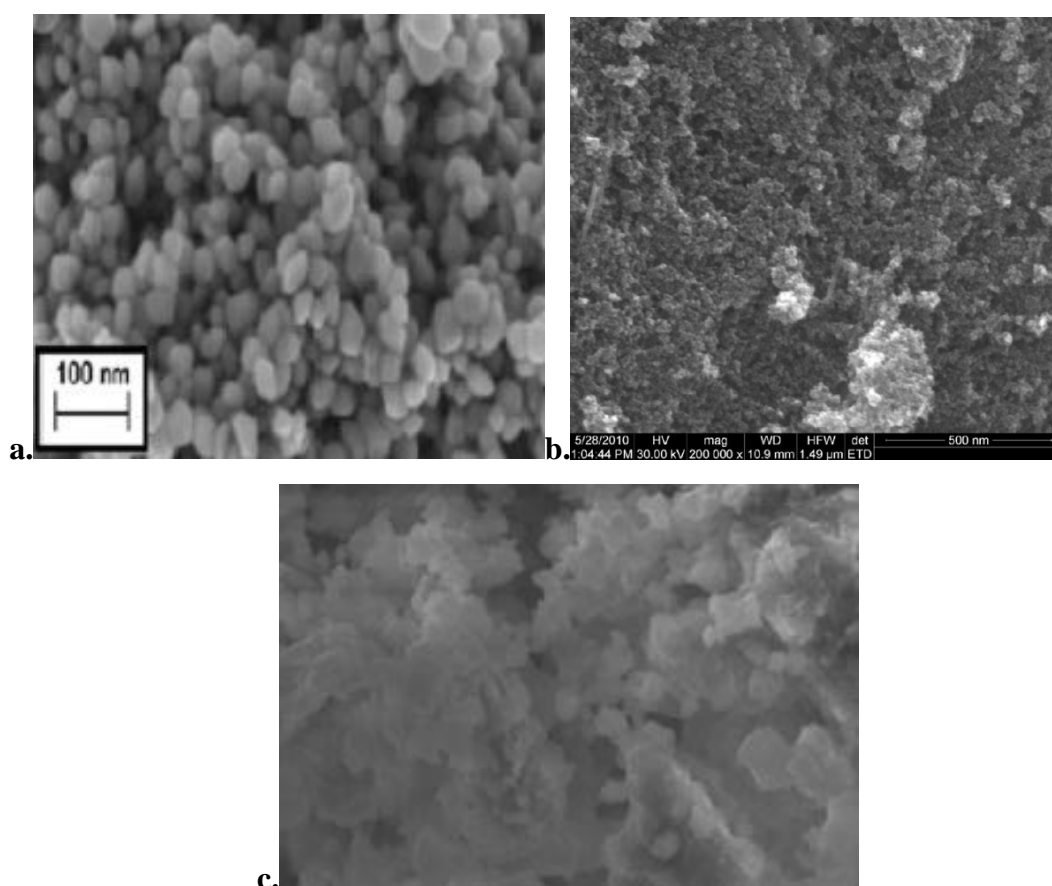
Figure 2.6: SEM Image of (a) α-Fe_2O_3 (Lassoued, et al., 2017), (b) γ-Fe_2O_3 (Gopal, et al., 2015) and (c) Fe_3O_4 (Prodan, et al., 2013)

TGA is a technical analysis used to monitor the change of mass of a substance varies with the temperature or time (Vyazovkin, 2012). On the other words, TGA can be defined by a technique used for heating a material and followed by inspection of the weight. A typical TGA system comprises of a sample pan which held up by

precision balance and remains in the furnace for heating or cooling during the experiment. The environment of the sample is usually controlled by a purge stream which may be inert gas that pass through the sample and exits through an exhaust (Chirayil, et al., 2017). Under the controlled temperature program, the program can be run in either isothermal system or non-isothermal system. The results of TGA are presented in thermogravimetric curve form. In addition, the shape and position of the thermogravimetric curve are varies with the mechanism and kinetics of the process related with the loss of the mass (Vyazovkin, 2012). Mishra, et al. (2014) reported that the TGA curve of iron oxide present around 3.0446% weight loss at temperature $180^{\circ}C$ due to the elimination of the water molecules absorbed by nanoparticles from atmosphere (Mishra, et al., 2014).

Fourier transform infrared spectrometry (FTIR) had been explored which significantly improved the performance of IR spectrometry to solve broader analytical problem (Bacsik, Mink and Keresztury, 2004). In FTIR, the infrared radiation is subjected to the sample and resulted part of the radiation had been absorbed by sample and the other part will transmit through the sample. The emitted radiation will form a spectrum which represents the molecules absorption and transmission. Due to the unique pattern, it suitably used in identification of all types of organic and many types of inorganic materials (Thermo Nicolet Corporation, 2001). Today, FTIR is mainly used for the identification of unknown material, determination of quality or consistency of a sample and determination of the component composition in a mixture (Gaffney, Marley and Jones, 2012). Mishra, et al. (2014) found that the presence of absorption bands in FTIR spectrum of iron oxide at 3354, 2359, 1621, 1033, 920 and 602 cm^{-1}. The absorption bands may be due to several bondings such as O-H stretching (3354 cm^{-1}), C–O bending (2359 cm^{-1}), N–H stretching and bending (1621 cm^{-1}), C–H stretching (1033 cm^{-1}) and vibrations of Fe– O bond (602 cm^{-1}).

2.5   Parameter Studies

2.5.1   Effect of Initial Dye Concentrations

The rate of photocatalytic degradation is mainly depends on the amount of dyes present in the solution. Kumar and Pandey (2017) reported that the photocatalytic degradation processes are contributed by the dyes which adsorbed on the catalyst surface but not in the bulk of the solution. They stated that initial concentration of dye played an

important role in the photocatalytic degradation efficiency and generally favoured at low dye concentration.

This could be explained by high amount of dye would adsorb on the surface of photocatalyst when the initial dye concentration was relatively high. Therefore, it might led to the insufficient available sites on the catalyst surface to generate ·OH, and consequently, the photocatalytic activity of catalyst was reduced (Gnanaprakasam, Sivakumar and Thirumarimurugan, 2015). Besides that, low efficiency degradation was due to the low excitation of electron from valance band to conduction band. The shorter path length for photons entering the solution was due to high initial dye concentration and finally reduce the amount of photon absorption on the photocatalyst (Hassena, 2016).
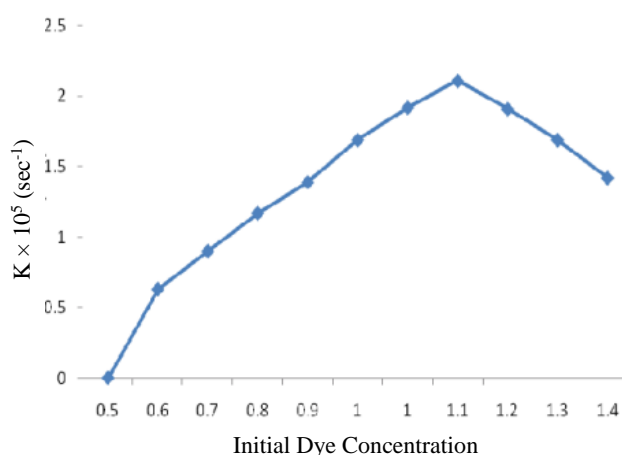
Figure 2.7: Effect of Initial Dye Concentration on the Photocatalytic Degradation Efficiency of Dye (Hassena, 2016)

2.5.2   Effect of Catalyst Dosage

The rate of photocatalytic reaction is generally directly proportional to the catalyst concentration. However, Reza, Kurny and Gulshan (2017) had reported that the catalyst concentration might provided a positive and negative impact on the photocatalytic degradation efficiency. Initially, the rate of degradation would increase as catalyst amount increase due to more active sites had been provided under high catalyst concentration and led to the high generation amount of ·OH (Gnanaprakasam, Sivakumar and Thirumarimurugan, 2015). At lower catalyst dosing rate, low degradation rate was reported might due to less amount of the irradiation of UV light had been absorbed by catalyst thus led to low photocatalytic degradation efficiency.

However, when catalyst dosing beyond a limit, it would had adversely effect on the degradation rate. At high catalyst dosing, penetration of photon flux in the reactor reduced and low degradation rate could be observed (Reza, Kurny and Gulshan, 2017). Besides that, excessive light scattering by the suspended particles might led to the decrement of the photocatalytic degradation efficiency as the opacity of the suspension had been increased. Last but not least, excessive concentration of catalyst would induce agglomeration of nanoparticles, reduce the surface area of the catalyst and also the number of surface active sites for the photocatalysis process (Gnanaprakasam, Sivakumar and Thirumarimurugan, 2015). Saratale, et al. (2014) investigated the performance of TiO_2 on phenol removal at different catalyst dosing rate. They found that extremely low phenol removal (44%) in the absence of the TiO_2. When catalyst dosing had increased from 0.5 to 2.0 g/L, high removal efficiency up to 98% could be observed. However, the catalyst dosing had continuous increased to between 4 to 6 g/L, the photocatalytic performance had become worst (Saratale, et al., 2014).

2.5.3 Effect of Solution pH

Reza, Kurny and Gulshan (2017) stated that the effect of pH on the efficiency of the photocatalysis reaction was very difficult. Depending on the nature of substrate and solution pH, there are several possible mechanisms will be occur during degradation such as ·OH attack, direct oxidation and direct reduction. The operating solution pH is crucial element in photocatalysis as it might affect the adsorption and desorption of organic pollutant on the catalyst surface and also the surface charge of the photocatalyst.

It shall be capable to predict the surface charge by comparing the pH with the isoelectric point (Kumar and Pandey, 2017). Thus, at higher solution pH, the surface of the photocatalyst is exist in negative charge and oppositely carries positive charge at the pH below isoelectric point. The negative charged surface of photocatalyst will more favour to the adsorption of cationic molecules due to the attraction between each other which lead to a high photocatalytic degradation efficiency. There is an opposite result as the removal of anionic organic molecules are more favourable at low solution pH due to the appearance of positive surface charge of catalyst. However, the degradation of pollutant was suppressed as the pH value exceed 12 due to the competition between ·OH and organic molecules to adsorb on the catalyst surface

(Gnanaprakasam, Sivakumar and Thirumarimurugan, 2015). Thus, the optimum operating solution pH for photocatalysis degradation is mainly depends on the nature of the pollutants.

The degradation of organic pollutant is not only contributed by photocatalytic process but also Fenton and Fenton-like processes because iron oxide are used as photocatalyst. Therefore, the determination of optimum pH will not only consider to achieve high photocatalytic degradation and also the efficiency of Fenton process. Meanwhile, as mentioned in section 2.3.1, the homogeneous Fenton process is only effective at an acidic pH condition which typically around from 3.0 to 4.0 (Deng and Zhao, 2015). However, with the introduction of heterogeneous system in Fenton process, it offer widely pH operating range to achieve high photocatalytic degradation efficiency which approximately around 2 to 7 (Xavier, et al., 2015).

2.6   Optimisation Study

Response surface methodology is now being used as a statistical which can reduces the workloads of research and form a suitable fit model for process optimisation than the conventional optimisation approaches. Therefore, RSM has been widely used in chemical engineering to find out the optimal point for many chemical operation (Sun, et al, 2019). RSM is a software which combine the mathematical and statistical function based on the fitting of empirical polynomial models (Bezerra, et al., 2008). The interaction between the independent process variable and their response are studied in RSM. The optimisation stage of RSM can be separated in few steps which are process variables screening, experiment design, response surface analysis and its evaluation which are mathematical and statistical analysis by using empirical models and the optimum response in terms of those parameters (Kataria and Garg, 2018). The mathematical relationship between the response and experimental parameters is shown by a non linear polynomial equation with constant term, linear terms, two-factor interaction terms and square terms which expressed as equation (2.24). A complete polynomial models consist of first-order terms, second-order terms and cross-product terms. This model produced by RSM can be used to predict the response with a parabolic curvature (Majdi, Esfahani and Mohebbi, 2019).

$$Y_{pred} = A_0 + A_1 x_1 + A_2 x_2 + A_3 x_3 + A_{12} x_1 x_2 + A_{13} x_1 x_3 + A_{23} x_2 x_3 \qquad (2.24)$$
$$+ A_{11} x_1^2 + A_{22} x_2^2 + A_{33} x_3^2$$

Central Composite Design (CCD) of RSM is utilised to determine the optimum condition of photocatalytic degradation of dyes by using green synthesised iron oxide. CCD is one of the function of RSM that are mostly are used to study a second order models by using design-Expert software. There are three levels for each factor in the optimisation which the high level (+1), low level (-1) and the center point (0) (Sktani, etl al, 2018). Therefore, the three independent parameters were set at specified levels. The maximum and minimum value for those parameters depend on the ability of the photocatalyst for removal of dyes (Sulaiman, et al., 2019). There are totally 20 runs are conducted at two levels with axial point ($\alpha = 1.68179$) on one response of photocatalytic degradation efficiency. Analysis of Variance are determined based on the suggested and modified models.

The F-values for analysis of variance (ANOVA) indicate the significance of the model terms for fitting the model. There are many parameters are used to determine quality of the model and how the experiment data are fit with the predicted value, for example, coefficient of determination (R^2), adjusted coefficient of determination (Adj. R^2), adequate precision, coefficient of variation (C. V.) and lack of fit (Li, et al., 2013). There are two main indicators of the model significance are R^2 and Adj. R^2 which found to be close to unity for good agreement between the result of experiment and prediction. For the F-value and small p-value indicate that the terms is considered in significance (Song, et al., 2016). Lack of fit indicates the ratio of the residual error to the pure error due to the replicated experiment results (Li, et al., 2013).

CHAPTER 3

METHODOLOGY AND WORK PLAN
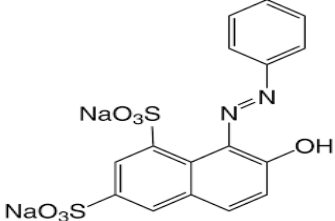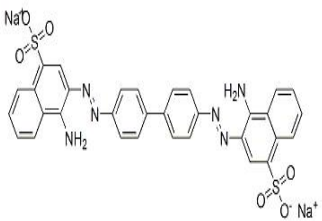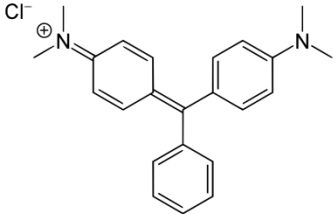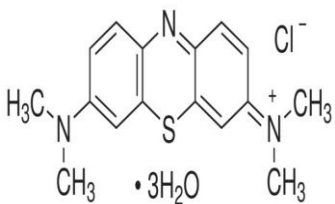
3.1 Materials and Chemicals

Table 3.1 lists the chemical reagents that are required in this experiment with their specifications. The chemical structure and properties of model pollutants are listed in Table 3.2.

Table 3.1: Chemicals Used in Experiment and Their Specifications

Chemical Reagent	Purity (%)	Brand	Usage
Acetic acid	80	Sigma-Aldrich	Synthesis of adsorbent and supported catalyst
Acid orange G	40	Sigma-Aldrich	Model pollutant
Congo red	97	R & M	Model pollutant
Hydrochloric acid (HCl)	37	Sigma-Aldrich	pH adjustment
H_2O_2	30	Sigma-Aldrich	Source of $\cdot OH$
Iron (III) nitrate nanohydrate $(Fe(NO_3)_3 \cdot 9H_2O)$	100	Merck & Co	Synthesis of iron oxide
Malachite green	99	Fisher Scientific	Model pollutant
Methylene blue	82	R & M	Model pollutant
Sodium hydroxide (NaOH)	97	Sigma-Aldrich	Synthesis of support based catalyst and pH adjustment

Table 3.2: Chemical Properties of Model Pollutants

Dye	Chemical Structure	Classification	Molecular Weight (g/mol)	Maximum Absorption Wavelength, λ (nm)
Acid orange G		Anionic, acid and azo	452.37	479
Congo red		Anionic, direct and diazo	696.67	498
Malachite green		Cationic, basic and triarylmethane	364.911	619
Methylene blue		Cationic, basic and thiazine	373.88	665

3.2　　Equipments

The apparatus required for this study are listed in Table 3.3 with their model. FTIR, SEM, TGA and XRD are used to characterise the synthesised iron oxide. Oven was used to prepare the adsorbent which were eggshell and eggshell membrane (ESM). Ultraviolet-visible (UV-vis) spectrophotometer were used in the analysis of the liquid samples. COD reactor was used to determine the COD value through reagent vials by heating the sample. pH meter was used to monitor the pH of solution and incubator shaker was used to provide stirring to the solution during the synthesis process.

Table 3.3: Model of Apparatus

Apparatus	Model
COD reactor	DRB200
FTIR	Bruker Alpha
ICP-OES	Optima 7000 DV
Incubator shaker	Labtech LSI-2016A
Oven	DHG-9023A
pH meter	Eutech PC300
SEM-EDX	Hitachi SEM Model S-3400
Spectrophotometer	DR3900
TGA	Tolendo TGA/DSC
Light source	500-W halogen lamp
UV-vis spectrophotometer	Jenway 6320D
XRD	Shimadzu XRD-600

3.3　　Overall Experiment Flowchart

Figure 3.1 shows that the flow chart of this experiment. In this study, preparation of peel extracts, treatment of eggshell and eggshell membrane had been first conducted. As the fruits peel extracts was prepared, they were used to synthesise iron oxide catalyst. The immobilization of iron oxide on adsorbents was conducted after the formation of iron oxide. The characterisation of support based iron oxide was done by FTIR, SEM, TGA and XRD analysis. In the next step, the process behaviour of photocatalytic degradation was studied by varying the dye concentration, catalyst dosage and pH of the solution. After that, the efficiency of the degradation was

determined by analysed the liquid samples through UV-vis spectrophotometer, COD analysis and ICP-OES.

```
┌─────────────────────────────────────┐
│  Preparation of orange peel extract  │
└─────────────────────────────────────┘
                  │
                  ▼
┌──────────────────────────────┐    ┌──────────────────────────────────┐
│ Synthesis of iron oxide       │    │ Preparation of eggshell and        │
│ particles                     │    │ eggshell membrane                  │
└──────────────────────────────┘    └──────────────────────────────────┘
                  │                               │
                  ▼                               ▼
          ┌──────────────────────────────────┐
          │ Immobilisation of iron oxide on   │
          │ support                           │
          └──────────────────────────────────┘
                          │
                          ▼
                ┌──────────────────────┐
                │   Characterisation     │
                │   • XRD                │
                │   • SEM                │
                │   • FTIR               │
                │   • TGA                │
                └──────────────────────┘
                          │
                          ▼
        ┌─────────────────────────────────────────────┐
        │         Process behaviour studies             │
        │ • Dye concentration (10, 20, 30, 40, 50 mg/L) │
        │ • Catalyst dosage (0.5, 1.0, 1.5, 2.0, 2.5 g/L)│
        │ • pH of solution (3, 5, 7, 9, 11)             │
        └─────────────────────────────────────────────┘
                          │
                          ▼
              ┌──────────────────────────────┐
              │   Liquid sample analysis       │
              │ • UV-vis spectrophotometer     │
              └──────────────────────────────┘
                          │
                          ▼
              ┌──────────────────────────────┐
              │      Optimisation Study        │
              └──────────────────────────────┘
```

Figure 3.1: Flow Chart of Experiment

3.4 **Experimental Setup**

Figure 3.2 shows the experiment setup. Hot plate and magnetic stirrer were used to provide proper mixing. Halogen lamp was used to emit some energy in UV region for photocatalytic reaction which held by retort stand.
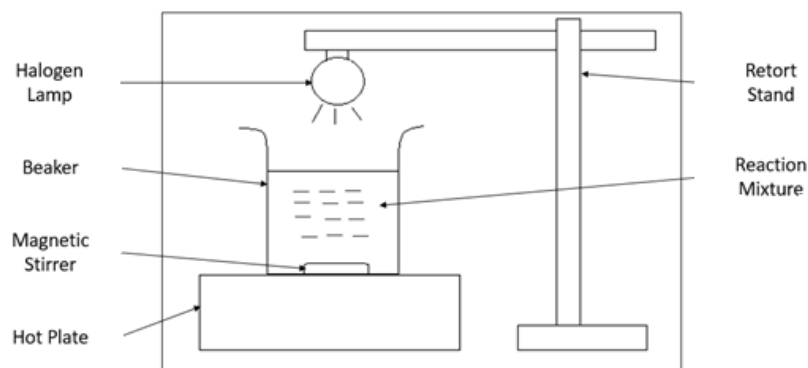
Figure 3.2: Schematic Diagram of Experimental Setup

3.5 **Preparation and Characterisation of Catalysts**

3.5.1 **Preparation of Fruit Peel Extracts**

Citrus aurantium (orange), Punica granatum (pomegranate), Malus domestica (apple) and Citrus limon (lemon) were first rinsed by using Milli-Q water. Next, the parts of coloured peels were intently removed from fruit by using knife and further cut into small size with the length about 0.5 cm and thickness was in between 5 to 6 mm. The chopped peels were cleaned using ultrasonic bath in double distilled water for 10 minutes and soaked in distilled water in weight ratio of 1:10. After 10 hours, the peels was filtered by a qualitative filter paper and the liquid extract was obtained.

3.5.2 **Preparation of Eggshell and Eggshell Membrane**

Discarded membrane-bounded eggshells were collected from food court and instantly stored in cold water. The eggshell is manually peeled off from the eggshell membrane and followed by immersed in an aqueous acetic acid solution for 2 days to further remove the remaining eggshell. Once eggshell completely being removed, rinsed with deionised water repeatedly in order to weaken the acidity and dried in an oven at 50ºC for 2 days. Grinding the eggshell and eggshell membrane was essential in order to transform it to powder form with high surface area.

3.5.3 Synthesis of Iron Oxide

500ml of 0.1 M of $Fe(NO_3)_3 \cdot 9H_2O$ was added into 100 ml of fruit peel extracts. The formation of iron oxide can be verified by indication of the colour change from yellow to black. The synthesis was conducted at room temperature. For pure iron oxide particles without catalyst support, 100ml of 2 M NaOH solution was added into the iron oxide suspension for precipitation of iron oxide particles.

3.5.4 Immobilisation of Iron Oxide

Firstly, 4.0 g of treated adsorbent was dissolved in 100 ml of distilled water which consist of 2% acetic acid solution. 600 ml of iron oxide suspension was then mixed with the eggshell powder solution. The mixture was dropped into a 2 M NaOH solution and kept stirring for 12 hours. Neutralization was conducted by washing the sample with ultrapure water and stored in a chemical bottle.

3.5.5 Characterisation

XRD is a technique used to determine the crystal structure through forming the XRD patterns. The XRD patterns of the samples were determined by using Shimadzu XRD-600 diffractometer with CuKα radiation (λ=1.5418 Å) as a sources. Before putting the sample, K-beta filter was utilised to remove the interference peak. After that, the sample was be placed into sample holder with smear uniformly onto a glass slide. The intensity data were collected continuously by controlled the diffraction pattern through emerging in the 2θ ranging from 20 to 80º with a step scan mode 0.001º/s. Besides, the topography and morphology of the sample could be obtained by SEM analysis. Before the analysis, the sample was fixed on the specimen holder by using double-sided adhesive tape. The acceleration voltage of 20 kV and magnification of 10, 20 and 40 kX were utilised to obtain high resolution image. EDX was utilised to determine the elemental composition of the sample. Meanwhile, the weight loss of the sample at different temperatures were observed from TGA analysis. In this study, TGA was conducted by increasing the heating temperature of sample which heating from 30ºC to 800ºC at a rate 10ºC/min. FTIR is an analysis that used to determine the functional group of organic or inorganic compound inside a sample. The spectrum of FTIR of sample was collected from 500 to 4000 cm^{-1} by using Bruker alpha FTIR spectrometer.

3.6   Preparation and Characterisation of Catalysts

Several operating parameters such as dye concentration, catalyst dosage and pH of solution were studied in order to investigate the efficiency of photocatalytic degradation.

3.6.1   Effect of Dye Concentration

In this section, five different dye concentrations at (20, 30, 40, 50, 60 mg/L) were studied. First of all, 20 mg/L of methylene blue in 100 ml of solution was added into a conical flask. pH of the solution was maintained at pH 7 which monitored by pH meter. 2.5 g/L of catalyst was added into the solution. After that, the solution was placed under the halogen lamp at room temperature. The sample was withdrawn from the flask for every 10 minutes in a duration of 1 hour analysis. The other four different concentrations were conducted at similar condition.

3.6.2   Effect of Catalyst Dosage

In this section, five different catalyst dosages of (0, 0.5, 1.0, 1.5, 2.0, 2.5 g/L) were studied. First of all, 20 mg/L of 100 ml of methylene blue solution was added into a conical flask. pH of the solution was maintained at pH 7 which monitored by pH meter. No catalyst was added into the solution for 0 g/L. After that, the solution was placed under the halogen lamp at room temperature. The sample was withdrawn from the flask for every 10 minutes in a duration of 1 hour analysis. The other five different dosages were conducted while keeping the parameter at a constant value.

3.6.3   Effect of Solution pH

The effect of solution pH on the degradation of wastewater by adjusting solution pH. Five different solution pH were tested which were 3, 5, 7, 9 and 11. The solution pH can be adjusted by dropping HCl or NaOH in the solution. 20 mg/L of methylene blue in 100 ml of solution was added into a conical flask and 2.5 g/L of catalyst was added. However, pH of solution was first adjusted to pH 3. After that, the solution was placed under the halogen lamp at room temperature. The sample was withdrawn from the flask for every 10 minutes in a duration of 1 hour for analysis. After that, the other four different solution pH were studied without changing the other parameter.

3.7 Liquid Sample Analysis

There are several liquid sample analysis were conducted to determine the residual concentration of dyes in the solution after degradation. The photocatalytic degradation efficiency was depended on the residual amount of dyes which remained in the solution. UV-vis spectrophotometer is one of the analytical technique used to determine the residual amount of organic dye to identify the absorption of the UV light by organic dye at the highest absorbance wavelength. According to Lambert-Beer law, the concentration of remaining dye was directly proportional to the absorbance of an organic pollutant. Therefore, the photocatalytic degradation efficiency was obtained by comparison of concentration before and after reaction.

3.8 Optimisation Study

Optimisation study was conducted by using Design Expert software. RSM is a software which consist of mathematical and statistical function. CCD of RSM was used to determine the relationship between those parameters and presented in three dimensional graph which the photocatalytic degradation efficiency as response in term of any two of the parameters. A total 20 sets of experiment was conducted and there are 6 runs was replicated. The ranges and level of parameters were determined through preliminary experiment which shown in Table 3.4.

Table 3.4: Actual Values of the Parameters and their Corresponding Coded Level in Central Composite Design

Parameters	Factors	Actual Values for the Coded Levels				
		$-\alpha$ (-1.68)	-1	0	+1	$+\alpha$ (+1.68)
Dye concentration, $[Dye]_o$ (mg/L)	x_1	13.18	20	30	40	46.82
Catalyst dosage, $[Fe_3O_4]_o$	x_2	1.16	1.5	2.0	2.5	2.84
pH	x_3	0.27	3	7	11	13.73

CHAPTER 4

RESULTS AND DISCUSSIONS

4.1   Characterisation of Iron Oxide

4.1.1   XRD Results

The crystallinity and phase structure of pure iron oxide, eggshell particles and iron oxide distributed on eggshell particles can be identified based on the result obtained from the XRD analysis. Figure 4.1 shows the XRD patterns for green synthesised pure iron oxide, eggshell particles and iron oxide distributed on eggshell particles. The synthesised iron oxide has characteristic peaks at $2\theta = 30°$, $35°$, $49°$, $63°$ and $78°$. Based on Figure 4.1, it could be observed that the XRD patterns for green synthesised iron oxide was similar to the magnetic Fe_3O_4 nanoparticles reported by Khatami, et al. (2019). The peaks at $30°$, $35°$, and $63°$ that were related to {220}, {311}, {440}, respectively. The iron oxide synthesised was appeared in black colour, which is the characteristic colour of Fe_3O_4 (Arsalani, et al., 2019).   Thus, with the similar characteristic observed in this study, it could be claimed that iron oxide were successfully produced by green synthesis method using orange peel.
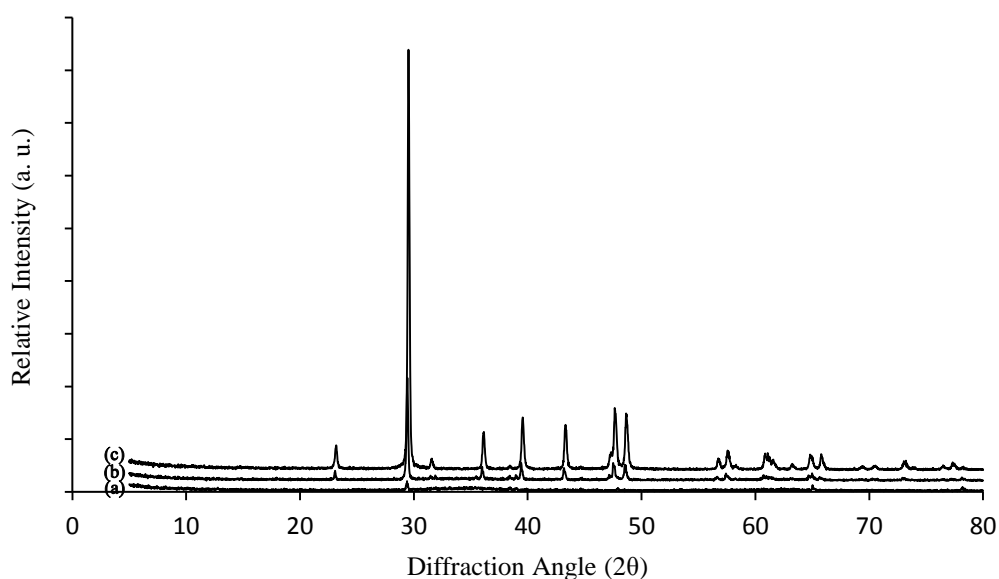

Figure 4.1: XRD Patterns for Green Synthesised (a) Pure Iron Oxide, (b) Iron Oxide Distributed on Eggshell Particles and (c) Eggshell Particles

Moreover, the characteristic peaks of iron oxide distributed on eggshell particles were shown at $2\theta = 23°, 30°, 36°, 39°, 43°, 47°, 48°, 57°, 65°, 78°$ which were similar to the characteristic peaks of eggshell particles. However, the intensity of the peaks of pure eggshell particles were higher than the peaks of iron oxide distributed on eggshell particles. This was due to the presence of iron oxide particles on eggshell particles surface. Besides, additional XRD diffraction peaks for iron oxide distributed on eggshell particles were identified as compared to the iron oxide. Ayodeji, et al. (2018) stated that the characteristic peaks of uncalcined eggshell at $2\theta = 29°, 36°, 39°, 44°, 47°, 48°$ were belong to calcium carbonate ($CaCO_3$) which were similar to the peaks of eggshell particles as shown in Figure 4.1(c) . In addition, it could be observed that the peaks at $29°, 36°, 48°, 65°$ and $78°$ were similar to the iron oxide. However, the intensity of the peak at $30°$ for iron oxide with support was extremely higher as compared to pure iron oxide. This was due to the small amount of iron oxide particles were distributed on eggshell particles.

The crystallite size of pure iron oxide and iron oxide distributed on eggshell particles could be determined by using Scherer's equation (2.23) with known full width at half maximum and diffraction angle. The calculated of crystallite size were based on the strongest peak found in the XRD patterns. Thus, the crystallite size of pure iron oxide and iron oxide distributed on eggshell particles were 49.75 nm and 56.08 nm, respectively. It could be observed that the crystallite size of iron oxide distributed on eggshell particles was slightly bigger than without distributed on eggshell particles, which was similar to the result that was obtained by Mosaddegh, Hosseininasab and Hassankhani (2015).

4.1.2   FTIR Results

The functional group and unknown materials can be identified based on the results obtained from the FTIR analysis. Figure 4.2 shows the FTIR spectra of green synthesised pure iron oxide with or without distributed on eggshell particles and eggshell particles. It could be observed that the characteristic absorption peaks of Fe-O band were found in the FTIR analysis of iron oxide and iron oxide distributed on eggshell particles which were located around 467.86 cm^{-1} and 471.94 cm^{-1}, respectively. These peaks were consistent with the spectra obtained by Radu, et al. (2017). The characteristic absorption peak at 834 cm^{-1} which found in analysis of iron oxide with and without distributed on eggshell particles was due to the C=O stretching

of amino (-NH$_2$) (Bharathi, et al, 2019). Besides, Wei, et al. (2012) stated that the peak at 1339 cm^{-1} and 1388 cm^{-1} were contributed to the vibration of the double covalent bond in –CH=CH–. Furthermore, the presence of absorption band at the range of 2340 cm^{-1} to 2360 cm^{-1} was observed due to the C-O bending (Mishra, et al., 2014). In this case, it might be due to the residue of organic extract that was remained on the catalyst surface.
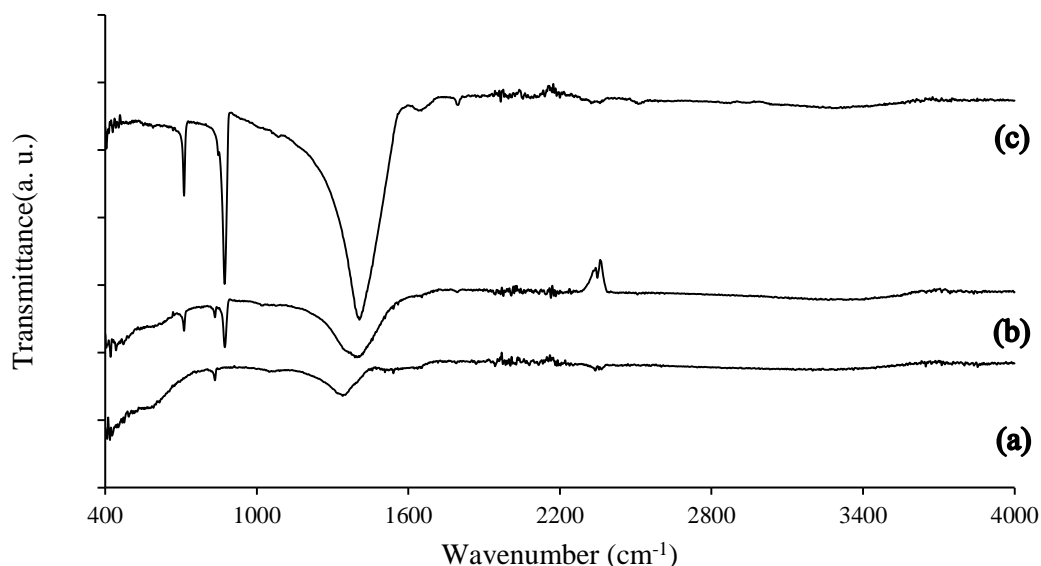
Figure 4.2: FTIR Spectra of Green Synthesised (a) Pure Iron Oxide, (b) Iron Oxide Distributed on Eggshell Particles and (c) Eggshell Particles

On the other hand, the absorption peak at 1406 cm^{-1} was found in eggshell particles which were attributed to the vibration of C-O bond in carbonate ion (CO$_3^{2-}$) from CaCO$_3$ presented on the eggshell particles (Kavitha, Geetha and Jacqueline, 2019). This characteristic peaks was also found in iron oxide distributed on eggshell particles. The absorption peaks at 712 cm^{-1} and 873 cm^{-1} was observed in the spectra of iron oxide distributed on eggshell particles and eggshell particles. The existence of these two peaks was due to the presence of eggshell support (Siriprom, 2018). Thus, it could be verified that the iron oxide particles was successfully distributed on the surface of eggshell particles.

4.1.3   SEM and EDX Results

The morphology of the pure iron oxide, iron oxide distributed on eggshell and eggshell particles are shown in Figure 4.3. It could be observed that pure iron oxide consist of majority spherical particles which was similar with the result obtained by Ruíz-Baltazar, et al. (2019). Besides, the average particle size of iron oxide particles was approximately in range from 0.1-1.0 µm. On the other hand, eggshell samples showed the porous structure which facilitated the distribution of iron oxide on the surface. High porosity structure of eggshell particles could provide more surface area to be distributed by iron (Nasrollahzadeh, Sajadi and Hatamifard, 2016). Furthermore, it could be observed that there are a lot of spherical particles were attached on the surface of high porosity structure. It verified that the iron oxide particles were being distributed on the surface of eggshell particles.
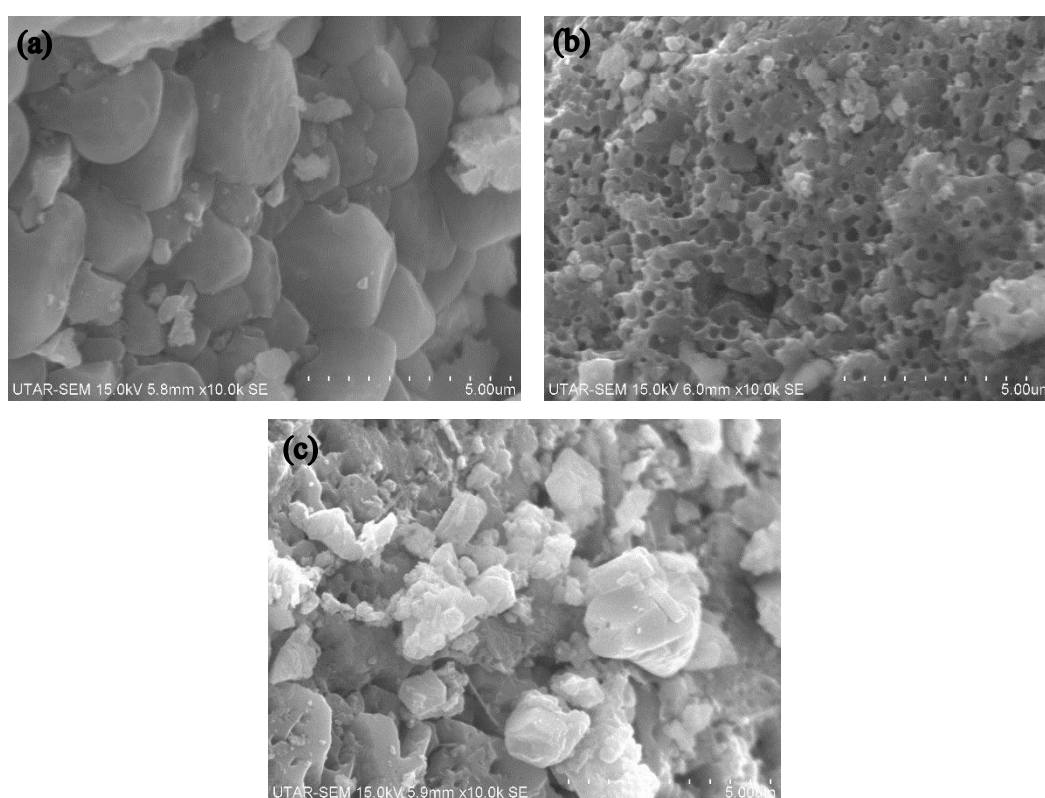

Figure 4.3: SEM Images of Green Synthesised (a) Pure Iron Oxide, (b) Eggshell Particles and (c) Iron Oxide distributed on Eggshell Particles

Table 4.1 shows the EDX analysis of pure iron oxide, eggshell particles and iron oxide distributed on eggshell particles. It could be observed that pure iron oxide

and iron oxide distributed on eggshell particles consist of the iron (Fe) and oxygen (O) element. The theoretical atomic ratio of Fe to O ratio were 0.75 and 0.667 for Fe_3O_4 and Fe_2O_3, respectively. Based on Table 4.1, the ratio of Fe and O for pure iron oxide and iron oxide distributed on eggshell particles were 0.55 and 0.19, respectively which closer to 0.667. The carbon (C) element might due to the residue of orange peel extract during the synthesis process. Meanwhile, high content of oxygen in the iron oxide with or without eggshell support resulted the ratio of Fe and O became lower than the theoretical value for Fe_3O_4 and Fe_2O_3 (Santos, et al, 2015). Furthermore, the presence of calcium (Ca) element was contributed by eggshell surface (Nasrollahzadeh, Sajadi and Hatamifard, 2016).

Table 4.1: EDX Results of Green Synthesised Pure Iron Oxide, Eggshell Particles and Iron Oxide Distributed on Eggshell Particles

Element	Atomic Percentage (At %)		
	Iron Oxide	Eggshell Particles	Iron Oxide Supported on Eggshell Particles
C	09.60	18.45	18.46
Fe	31.91	-	10.94
O	58.49	53.14	57.58
Ca	-	28.14	13.01

4.1.4 TGA Results

Thermogravimetric analysis is generally used to characterise a substance by determining the changes of physico-chemical properties at elevated temperature (Coats and Redfern, 1963). Figure 4.4 shows that the weight loss of iron oxide distributed on eggshell particles and heat flow obtained by TGA analysis. It could be observed that the total weight loss of iron oxide distributed on eggshell particles was around 37 % and the heat flow curve showed that endothermic and exothermic reaction were involved. Based on the weight loss curve, two stages were observed.

There was about 15 wt% weight loss was observed from temperature of 50 °C to 300 °C. This was due to desorption and evaporation of surface water molecules (Yadav, 2018). The water molecules on the particles surface absorbed heat to desorb and evaporate. It could be observed that the heat flow decreased in this stage, this could

be explained by the energy generated was gained by water molecules for desorption and evaporation. Besides, Nasrollahzadeh, Sajadi and Hatamifard (2016) also stated that the decomposition of the residue organic content (orange peel) was occurred on the particles surface at temperature from 150°C to 240°C.

The second stage was about 22 wt% weight loss at elevated temperature from 300 °C to 700 °C, which corresponding to the combustion of inorganic and organic molecules. Thus, exothermic reaction could be observed with heat flow were dramatically increased. Besides, the weight reduction at this temperature might also due to the phase transformation of Fe_3O_4 (Nikitin, et al., 2019). This situation was consistent with the results obtained by Esmaeilnezhad, Karimian and Choi (2019). Furthermore, $CaCO_3$ started to decompose at temperature above 660 °C, therefore, the total weight was slightly decreased (Nasrollahzadeh, Sajadi and Hatamifard, 2016). Since the decomposition of $CaCO_3$ were endothermic reaction, the heat flow was decreased at temperature from 660°C. Moreover, Gollakota, Volli and Shu (2019) stated that the removal of surface physisorbed water, calcium hydroxide ($Ca(OH)_2$) might contributed to the weight loss at temperature of 408.2°C and 659.1°C.
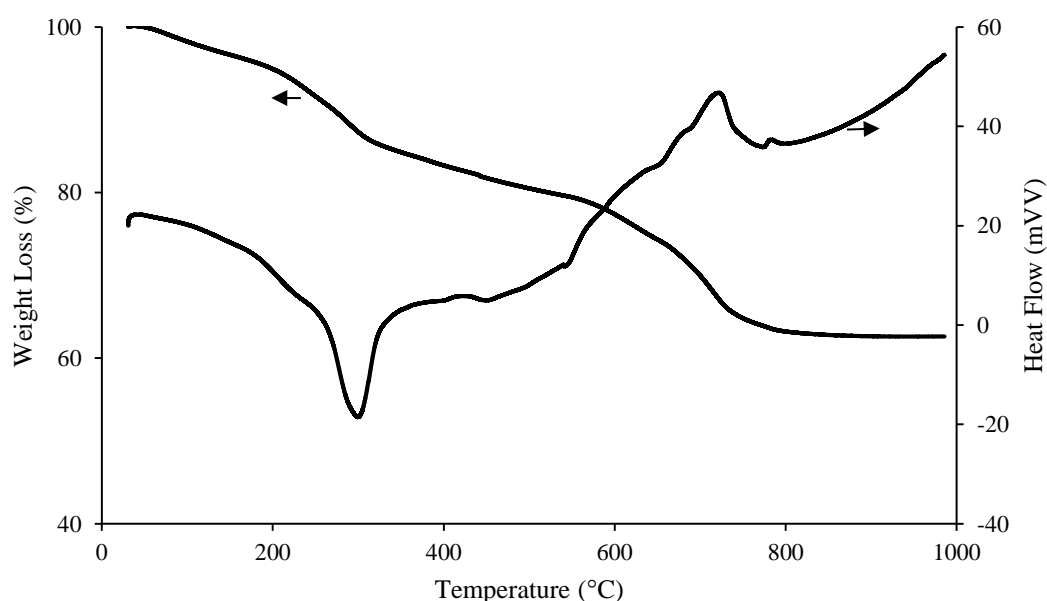
Figure 4.4: Thermogravimetric Curve of Green Synthesised Iron Oxide Distributed on Eggshell Particles

4.2 Adsorption and Photocatalytic Degradation

Figure 4.5 shows the removal of Congo red by using pure iron oxide, eggshell particles and iron oxide distributed on eggshell particles through adsorption or photocatalytic degradation. The main difference between both processes was the presence of the halogen lamp during degradation for photocatalytic degradation whereas the adsorption was conducted in the dark condition. It could be observed that photocatalytic degradation by using iron oxide distributed on eggshell particles had the higher photocatalytic degradation efficiency. However, the photocatalytic degradation of Congo red by using pure iron oxide had the lower photocatalytic degradation efficiency.
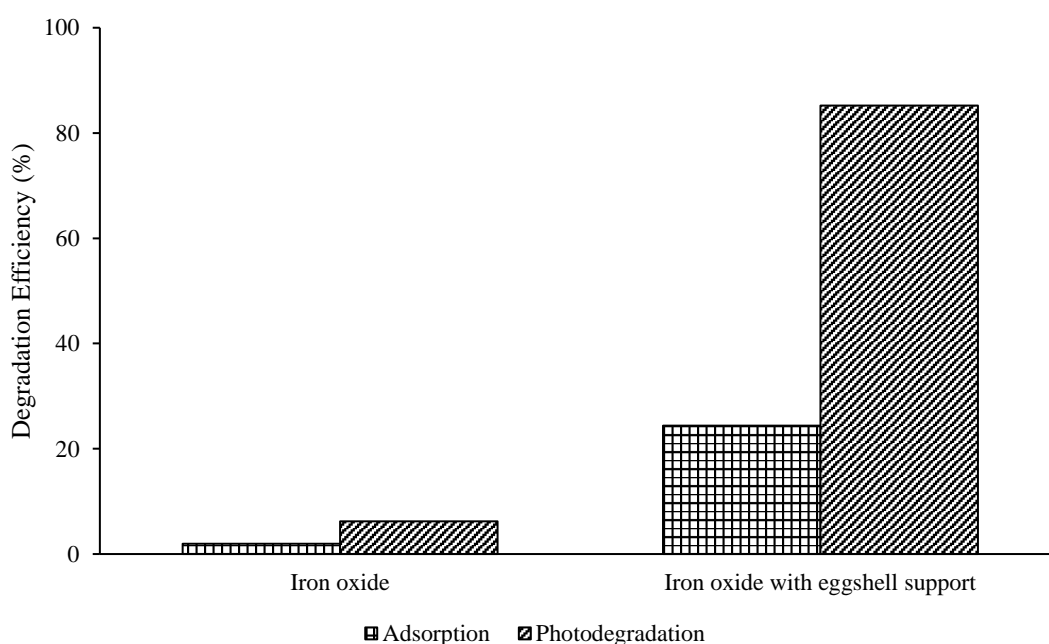
Figure 4.5: Concentration of Congo Red versus Time for Adsorption or Photocatalytic Degradation (Initial Dye Concentration = 20 ppm, Catalyst Dosage = 2.5 g/L, Solution pH = 7)

Iron oxide distributed on eggshell particles showed higher photocatalytic degradation efficiency for both adsorption and photocatalytic degradation processes. This might be due to the presence of high porosity structure of the eggshell particles. Since eggshell consist of macroporous network structure, iron oxide particles would easily distributed on the eggshell surface. Thus, large contact area and distributed particles would led to a better catalytic activity on the reduction of dye concentration

(Laca, Laca and Diaz, 2017). Besides, the ability for adsorption using eggshell particles could not be ignored. Tsai, et al. (2008) utilised the eggshell waste as an adsorbent for dye degradation and demonstrated a considerable removal efficiency. Thus, it could be observed that the adsorption conducted by iron oxide distributed on eggshell particles was higher than that of without eggshell support. Moreover, Kadirove, et al. (2013) also stated that the adsorption was possibly occurred during photocatalytic degradation of dyes.

4.3 Parameter Studies

4.3.1 Effect of Dye Concentration

The effect of Congo red concentration (10, 20, 30, 40 and 50 ppm) on the performance of photocatalytic degradation of Congo red is shown in Figure 4.6. It was observed that the photocatalytic degradation efficiency of 10 ppm concentration of dye was nearly 100% and decreased to 58 % while increasing dye concentration to 50 ppm. Besides, it could be observed that photocatalytic degradation efficiency was dramatically increased in first 10 minutes and followed by slightly increased in the next 50 minutes. It was interesting to note that the degradation efficiencies of dye with concentration of 40 ppm and 50 ppm were almost the same.

The photocatalytic degradation efficiency decreased as the dye concentration increased. This was due to more dye molecules adsorbed on the catalyst as the amount of dye increased. Thus, the surface space of iron oxide would being occupied and affect the generation of $\cdot OH$ (Ebrahimi, et al., 2019). Besides, high dye concentration would increase the opacity of dye solution, which might absorb more light than the catalyst. Consequently, this reduced the excitation of iron oxide particles due to the low number of photon that reached to the catalyst surface (Pouretedal, et al., 2009). As mentioned previously, the photocatalytic degradation efficiency of 40 ppm and 50 ppm were approximately the same value due to the saturation condition. When all iron oxide particles were occupied by the dye molecules, the photocatalytic degradation efficiency would drop which was consistent to the result obtained by Madhura and Gayathri (2019).

In conclusion, the lower the initial dye concentration, the higher the photocatalytic degradation efficiency of dyes. Thus, the initial dye concentration of 10 ppm showed the highest photocatalytic degradation efficiency.
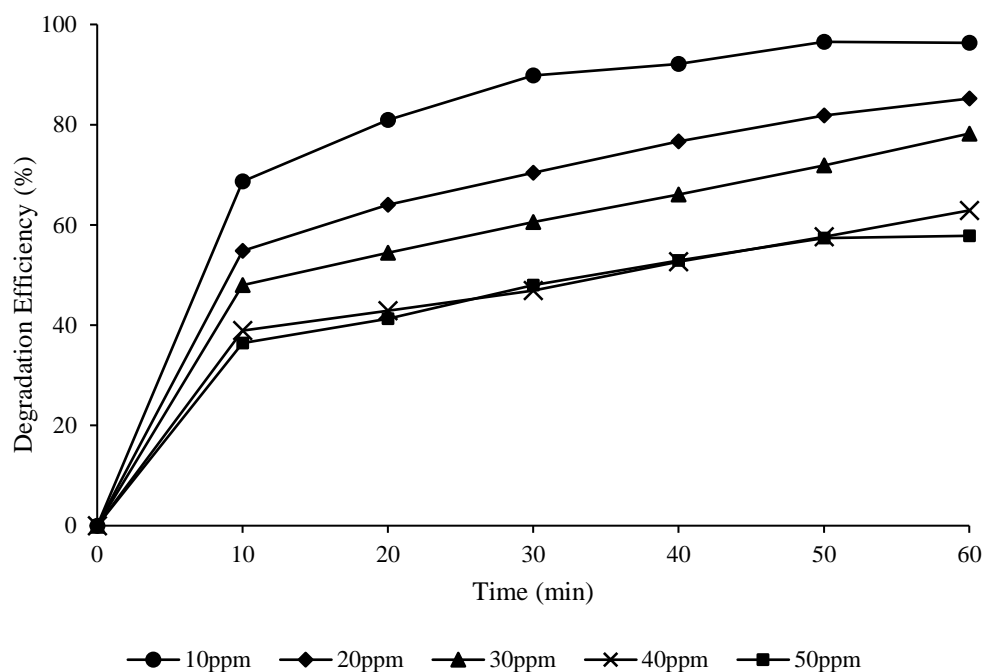
Figure 4.6: Effect of Congo Red Concentration on the Photocatalytic Degradation of Congo Red (Catalyst Dosage = 2.5 g/L, Solution pH = 7)

4.3.2 Effect of Catalyst Dosage

Figure 4.7 indicates the effect of catalyst dosage (0.5, 1.0, 1.5, 2.0 and 2.5 g/L) on the photocatalytic degradation efficiency of Congo red. It could be observed that the photocatalytic degradation efficiency was directly proportional to the catalyst dosing. As the amount of iron oxide involved in the reaction increased, the higher the photocatalytic degradation efficiency. Among those catalyst dosage, 2.5 g/L of iron oxide demonstrated the highest photocatalytic degradation efficiency. The photocatalytic degradation efficiencies of Congo red in the presence of halogen lamp for 0.5, 1.0, 1.5, 2.0 and 2.5 g/L of iron oxide were 28%, 39%, 65%, 73% and 85%, respectively.

The higher the catalyst dosage, the higher the photocatalytic degradation efficiency. This results could be explained by the increment of active sites available for the photocatalytic degradation process (Shi, et al., 2018). Since high amount of catalyst were used, the amount of Fe^{2+} and Fe^{+3} also increased, which were attributed to produce more $\cdot OH$ to degrade organic dyes (Zhang, et al., 2008). The same trend of the results was reported by Fu, et al. (2019) whose had investigated the dosing of α-Fe_2O_3 on the photocatalytic degradation of acetochlor. However, Anju Chanu, et al. (2019) stated that excessive amount of catalyst dosage would led to adverse effect on

the photocatalytic degradation efficiency. In this case, particles agglomeration would happened and increased turbidity of the dye solution, this inhibited the penetration of the light due to scattering effect (Ebrahimi, et al., 2019).

In short, the photocatalytic degradation efficiency could be improved by increasing the iron oxide dosage. The highest efficiency could be achieved by using amount of catalyst of 2.5 g/L.
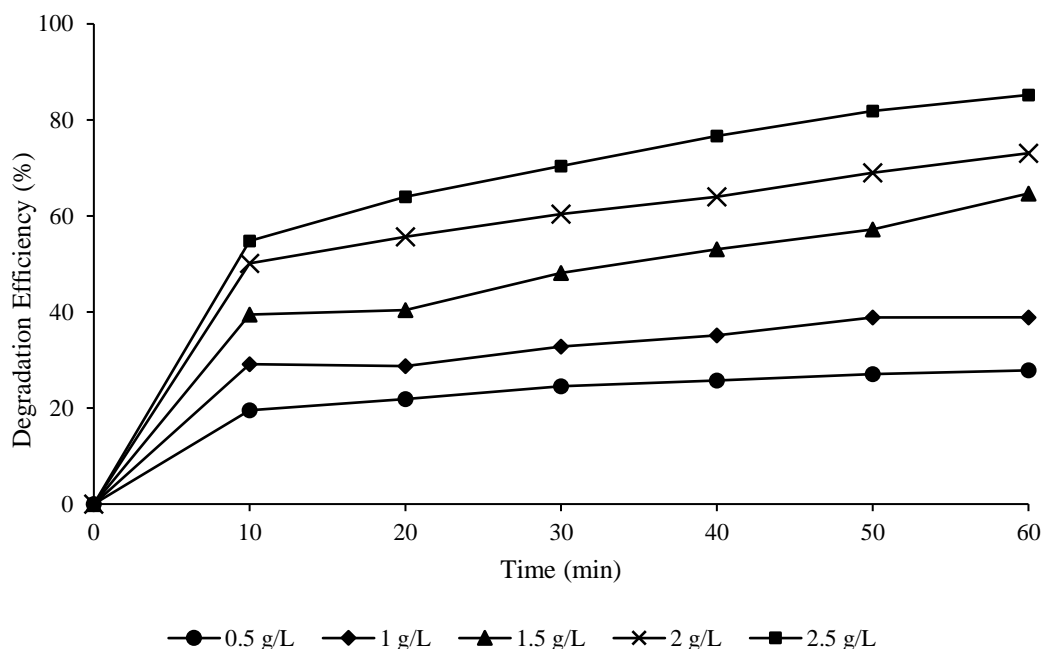
Figure 4.7: Effect of Catalyst Dosing on the Photocatalytic Degradation of Congo Red (Initial Dye Concentration = 20 ppm, Solution pH = 7)

4.3.3 Effect of Solution pH

The effect of solution pH on the photocatalytic degradation of Congo red was investigated as shown in Figure 4.8. Based on the graph, the photocatalytic degradation efficiency was inversely proportional to the solution pH. Among five solution pH, the photocatalytic degradation efficiency at solution pH 3 and pH 5 showed the highest removal of dyes with approximately 91 %. The degradation efficiencies for solution pH value of 3, 5, 7, 9 and 11 were 91 %, 91 %, 85%, 73 % and 44 %, respectively.

The photocatalytic degradation efficiency increased as the solution pH decreased. This was because of the negatively charged of photocatalyst surface in alkaline condition might repelled the organic dye molecules, thus, reduced the adsorption of dye molecules on catalyst surface (Nezamzadeh-Ejhieh and Ghanbari-

Mobarakeh, 2015). Besides, Ahmed, Yaakob and Akhtar (2016) stated that the formation of relatively inactive ferryl ions (FeO^{2+}) would reduce the photocatalytic reaction rate. Higher solution pH value would also led to the decomposition of H_2O_2 into H_2O and O_2, which was unstable compounds. Since the amount of H_2O_2 reduced, the ·OH produced would decreased, thus, lower the photocatalytic degradation efficiency. The similar results were reported by Karimi, Zohoori and Yazdanshenas (2014) whom found that the photocatalytic degradation efficiency was gradually decreased with increasing solution pH value.
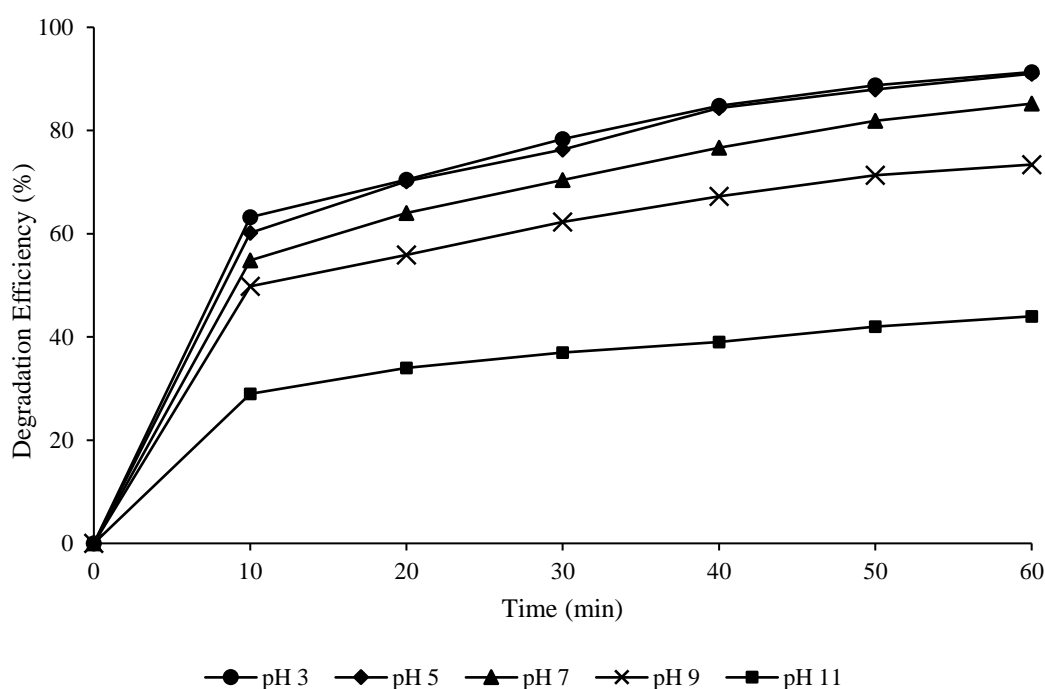
Figure 4.8: Effect of Solution pH on the Photocatalytic Degradation of Congo Red (Initial Dye Concentration = 20 ppm, Catalyst Dosage = 2.5 g/L)

4.4   Optimisation Study

4.4.1   Regression Analysis

Response surface methodology was utilised to determine the interaction effects between three independent parameters through a central composite design. The overall photocatalytic degradation efficiency of Congo red was found in the range of 1.5 % to 91.1%. The condition of experiment runs, the experimental and predicted values of photocatalytic degradation efficiency are shown in Table 4.2. Equation (4.1) was

obtained by using regression analysis, which expressed the relationship between photocatalytic degradation efficiency and those independent parameters. The equation was expressed by the predicted photocatalytic degradation efficiency in term of several parameters such as initial dye concentration (x_1), catalyst dosing (x_2) and pH value (x_3). The positive and negative sign of the coefficient indicated that increment or decrement effect on the photocatalytic degradation efficiency respectively.

$$Y_{pred} = 57.2467 - 12.3317x_1 + 9.87543x_2 - 21.0472x_3 + 2.9375x_1x_2 \qquad (4.1)$$
$$-0.9875x_1x_3 - 3.1625x_2x_3 - 1.58841x_1^2 + 1.4769x_2^2$$
$$-7.75084x_3^2$$

The ANOVA results are shown in Table 4.3. The proportion of variation could be observed from ANOVA results, which based on the value of determination coefficient (R^2). Based on the result, the predicted and adjusted R^2 were both 99% (close to unity), which implied that this model was sufficient for the regression data. In other words, 99 % of photocatalytic degradation efficiency could be explained by this model, and, only 1% of the deviation of response could be found. In short, high value of R^2 indicated high consistency results between the response and those independent parameters.

The overall validity of the model was depend on the model F-value. The model F-value was 798.39 which indicated that the model was significant and there was only 1% of chance that the F-value might occurred due to noise. Therefore, the regression model for this photocatalytic degradation was found to be highly significant. Besides, the adequate precision ratio was measured by the signal to noise ratio. The adequate precision of this quadratic model of photocatalytic degradation was 107.22, which was greater than 4. Therefore, it indicated that an adequate signal could be utilised to navigate the design space. The lack of fit F-value was 3.70, which implied that pure error was not significant. There was only 8.86 % of chance that a lack of fit F-value could occurred due to noise.

The p-value was the probability of the observed F-value if the null hypothesis was true. Small value of probability was required to reject the null. The value of probability was the integration of the area, which located under the curve of the F-distribution that lied beyond the observed F-value (Pang, Abdullah and Bhatia, 2011).

Table 4.2: Experiment Design Conditions and Their Respective Photocatalytic Degradation Efficiency

Standard Order	Point Type	Coded Independent Variable Levels			Degradation Efficiency, % (y)	
		$[Dye]_0$, mg/L (x_1)	$[Fe_3O_4]_0$, g/L (x_2)	pH	Experimental Values	Predicted Values
1	Fact	20 (-1)	1.5 (-1)	3 (-1)	72.1	71.68
2	Fact	40 (1)	1.5 (-1)	3 (-1)	43.7	43.11
3	Fact	20 (-1)	2.5 (1)	3 (-1)	91.1	91.88
4	Fact	40 (1)	2.5 (1)	3 (-1)	75.1	75.06
5	Fact	20 (-1)	1.5 (-1)	11 (1)	37.1	37.88
6	Fact	40 (1)	1.5 (-1)	11 (1)	5.4	5.37
7	Fact	20 (-1)	2.5 (1)	11 (1)	44.1	45.43
8	Fact	40 (1)	2.5 (1)	11 (1)	23.5	24.67
9	Axial	13.18 (-1.68)	2 (-1)	7 (-1)	74.6	73.49
10	Axial	46.82 (1.68)	2 (0)	7 (0)	31.96	32.01
11	Axial	30 (0)	1.16 (-1.68)	7 (0)	44.3	44.82
12	Axial	30 (0)	2.84 (-1.68)	7 (0)	79.6	78.03
13	Axial	30 (0)	2 (0)	0.2728 (-1.68)	70.2	70.72
14	Axial	30 (0)	2 (0)	13.73 (1.68)	1.5	0
15	Center	30 (0)	2 (0)	7 (0)	55.9	57.25
16	Center	30 (0)	2 (0)	7 (0)	56.9	57.25
17	Center	30 (0)	2 (0)	7 (0)	57.9	57.25
18	Center	30 (0)	2 (0)	7 (0)	57.4	57.25
19	Center	30 (0)	2 (0)	7 (0)	57.1	57.25
20	Center	30 (0)	2 (0)	7 (0)	58.1	57.25

Therefore, the significance of the terms of the model was measured by the p-value which smaller than 0.05. However, if the value was greater than 0.1 indicated that the model terms were not significant to the model developed. If the number of insignificant terms were higher, it could be improved by model reduction as well. Based on the analysis, it could be concluded that all the model terms were significant including individual terms (x_1, x_2 and x_3) and interaction terms (x_1x_2, x_2x_3 and x_1x_3).

Table 4.3: ANOVA Results for Photocatalytic Degradation Efficiency of Congo Red

Factors	Squares Sum	Freedom Degrees	Square Average	F-value	Probability p-value	
Quadratic model	10569.85	9	1174.43	798.39	<0.0001	significant
x_1	2076.79	1	2076.79	1411.82	<0.0001	
x_2	1331.87	1	1331.87	905.42	<0.0001	
x_3	6049.8	1	6049.8	4112.71	<0.0001	
x_1x_2	69.03	1	69.03	46.93	<0.0001	
x_1x_3	7.80	1	7.80	5.30	0.0430	
x_2x_3	80.01	1	80.01	54.39	<0.0001	
x_1^2	36.36	1	36.36	24.72	<0.0001	
x_2^2	31.43	1	31.43	21.37	0.0002	
x_3^2	865.77	1	865.77	588.56	<0.0001	
Residual	14.71	10	1.47			
Lack of fit	11.58	5	2.32	3.70	0.0886	Not significant
Pure error	3.13	5	0.6257			
Corrected total	10584.56	19				

$$R^2 = 0.99; \text{ adequate precision} = 107.22$$

Figure 4.9 shows the actual and predicted values of photocatalytic degradation of Congo red. It could be observed the value of the points were mostly located on the line, which represented experiment values were in good agreement with the predicted model. It could be concluded that the developed model was suitable to explain the photocatalytic degradation of Congo red in the studied range.
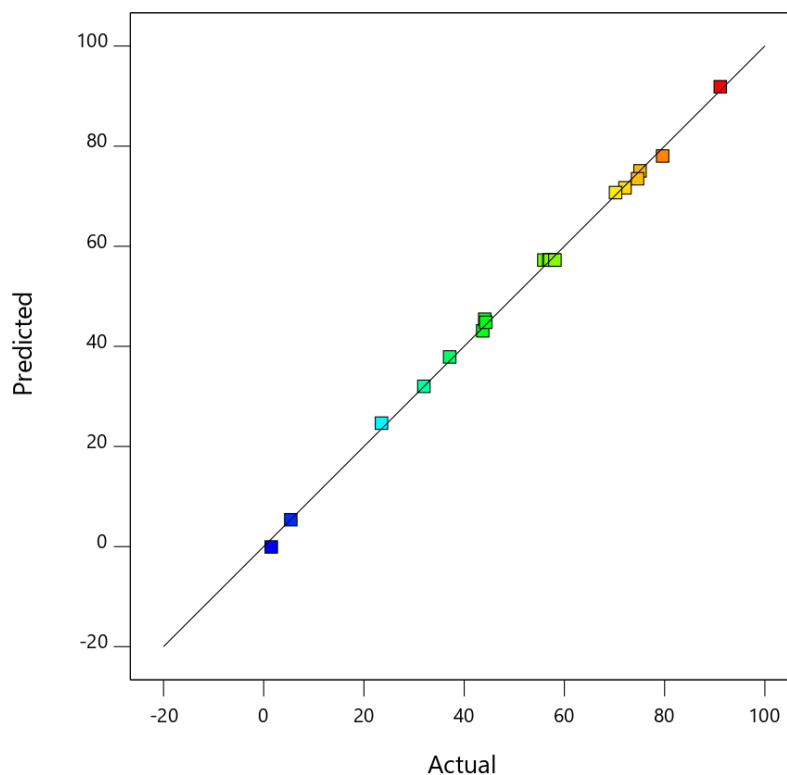
Figure 4.9: Actual and Predicted Values of Photocatalytic Degradation of Congo Red ($R^2 = 0.99$)

4.4.2 Response Surface Analysis (RSM)

Through RSM optimisation program, the interaction between three parameters had been determined. Photocatalytic degradation of Congo red was normally affected by three main factors, which were initial dye concentration (x_1), catalyst dosage (x_2) and solution pH (x_3), their corresponding higher order terms (x_1^2, x_2^2 and x_3^2) and also the interaction between three of them (x_1x_2, x_1x_3 and x_2x_3). The effect of the initial dye concentration and catalyst dosage on photocatalytic degradation efficiency is shown in the Figure 4.10. It could be observed that the amount catalyst dosage was increased with increment of dye concentration until it reach an optimum point.

The photocatalytic degradation efficiency of Congo red was reduced with increasing the initial dye concentration with different catalyst dosage. This was because the increment of dye molecules would tend to adsorb on the catalyst surface, thus, it inhibited the generation of ·OH to attack this huge amount of dye molecules (Warkhade, et al., 2019). This was consistent to the result studied previously (Ebrahimi, et al., 2019). With constant dye concentration, the photocatalytic degradation

efficiency was increase with higher catalyst dosing. This was due to high amount of ·OH were generated for photocatalytic degradation of Congo red (Shi, et al., 2018).
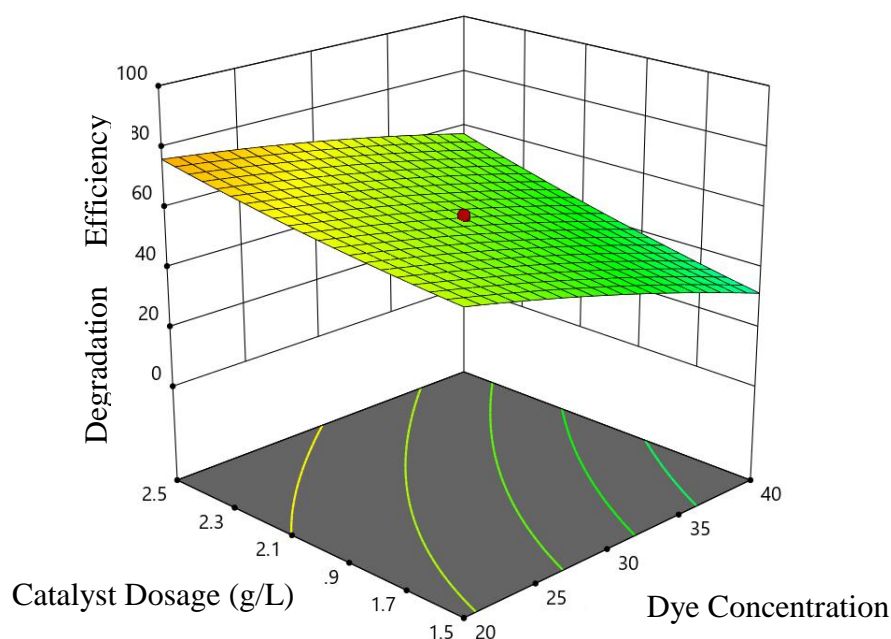

Figure 4.10: Effect of Initial Dye Concentration and Catalyst Dosage on the Photocatalytic Degradation Efficiency of Congo red at solution pH 7

Three-dimensional response surface plot of the interaction between initial dye concentration and solution pH at constant catalyst dosage is shown in Figure 4.11. It could be observed that solution pH was playing an important role on the photocatalytic degradation of Congo red. The photocatalytic degradation efficiency of Congo red was higher in acidic environment. The photocatalytic degradation efficiency of Congo red increased as the initial dye concentration are decreased. By comparing the results in run 3 and 8, it indicated that the optimum efficiency could be achieved easily by lowering the initial dye concentration and solution pH. This was due to negatively charged surface photocatalyst in alkaline condition which would repel those anionic dyes molecules that were trying to adsorb on its catalyst surface (Hassena, 2016). Besides, under alkaline condition, FeO^{2+} were formed and reduced the amount of Fe^{2+} and Fe^{3+} (Ahmed, Yaakob and Akhtar, 2016). Consequently, the amount of ·OH produced were not sufficient for large amount of dye molecules. Thus, the photocatalytic degradation efficiency of high dye concentration under alkaline condition showed the lowest performance.
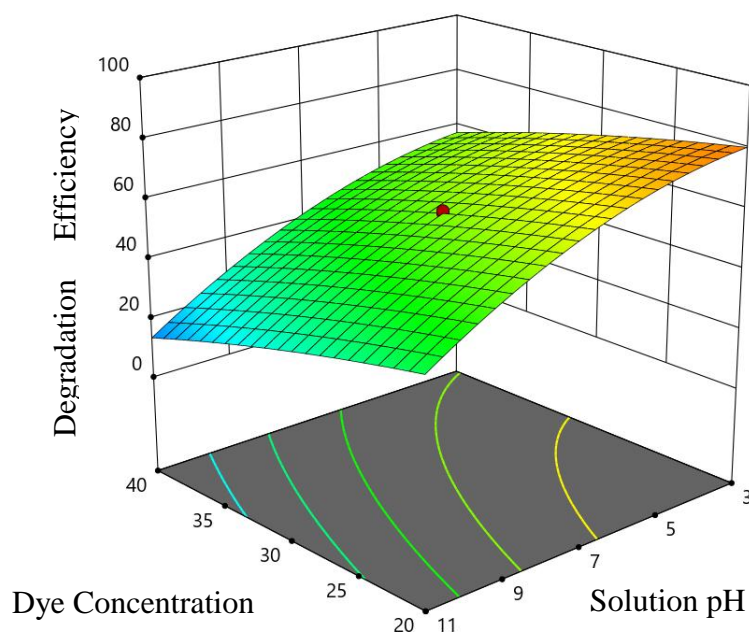
Figure 4.11: Effect of Initial Dye Concentration and Solution pH on Photocatalytic Degradation Efficiency of Congo Red at Catalyst Dosage of 2.0 g/L

Figure 4.13 shows the effect of solution pH and catalyst dosage on the photocatalytic degradation of Congo red. Based on the plotted graph, the optimum photocatalytic degradation efficiency could be achieved by lowering solution pH value and increased the catalyst dosage. Besides, it could be observed that the interaction between solution pH and catalyst dosing were not significant as compared to the other two interactions. Under constant solution pH, the variation of catalyst dosage from 1.5 g/L to 2.5 g/L were not play obvious effect on the photocatalytic degradation efficiency, the increment was approximately less than 15 %. However, the increment of photocatalytic degradation efficiency with increased catalyst amount under pH 3 condition were more than 25 %. This could be explained by the generation of inactive FeO^{2+} and iron (II) hydroxide ($Fe(OH)_2$), which unable to produce ·OH. Although the amount of catalyst was increased, the generation of ·OH by Fe^{2+} or Fe^{3+} were prohibited (Ahmed, Yaakob and Akhtar, 2016). More generation of ·OH at acidic condition, therefore, the photocatalytic degradation efficiency was significantly increased while increasing the catalyst dosing amount.

In conclusion, the photocatalytic degradation efficiency of Congo red increased when utilising low initial dye concentration, high catalyst dosage low solution pH.

Besides, the photocatalytic degradation efficiency could be improved by the immobilisation of catalyst on the surface of support such chitosan, eggshell. High surface area, robust and stable structure were the properties of the support, which able to improve the reaction rate (Martins, et al., 2017).
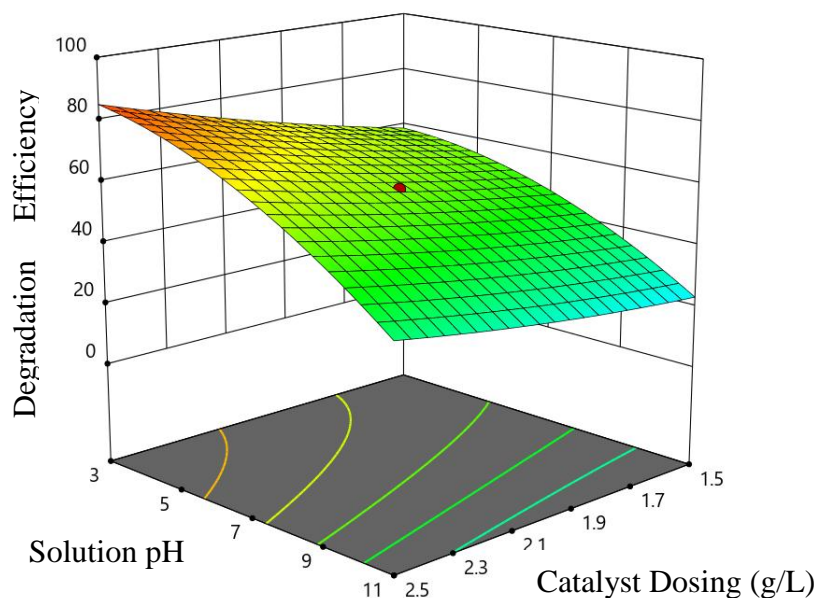
Figure 4.12: Effect of Solution pH and Catalyst Dosage on the Photocatalytic Degradation Efficiency of Congo Red at Initial Dye Concentration of 30 ppm

4.4.3 Model Validation and Experimental Confirmation

According to several researches, the highest possible photocatalytic degradation efficiency was obtained by optimising three independent variables by using RSM. Besides, Design of Expert (DOE) software was used to generate a few solutions by referring to the order of suitability to optimise variables and verify the predicted model. Five solutions were selected as optimum conditions. The accuracy of the photocatalytic degradation efficiency were calculated and the difference results between experimental and predicted values were within 1.5 % as shown in Table 4.4.

The conditions at initial concentration of Congo red of 20.422 ppm, pH value of 3.197, and catalyst dosage amount of 2.498 g/L were selected for the process variables optimisation. The experimental value of the photocatalytic degradation efficiency of Congo red was 92.361 % and the value is closer to the predicted value, which is 91.213 % as shown in Table 4.4. In addition, the good results of experiment values confirmed that the efficiency of the RSM method to optimise the photocatalytic

degradation of Congo red was reliable. The changes in the absorption spectrum of Congo red during photocatalytic degradation is demonstrated in the Figure 4.13. The photocatalytic degradation of Congo red was justified by the significant drop in the absorbance of the highest peak.

Table 4.4: Experiment and Predicted Results for Model Validation which Conducted at Optimum Conditions

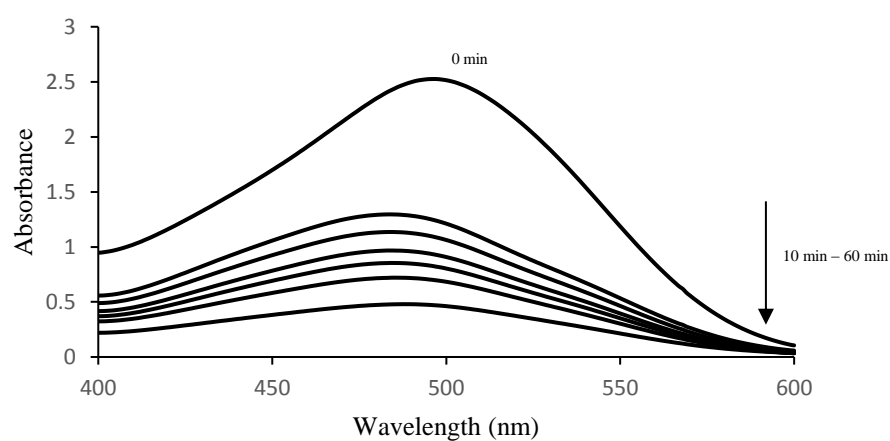| Runs	x_1	x_2	x_3	Experimental values	Predicted values
1	20.753	2.494	3.002	88.15	91.32
2	20.13	2.497	3.156	86.11	91.43
3	20.327	2.493	3.064	88.06	91.39
4	20.422	2.498	3.197	92.36	91.21
5	21.167	2.498	3.001	95.96	91.20

Figure 4.13: Absorbance Value versus Wavelength during Photocatalytic Degradation of Congo Red (Initial dye concentration = 20.422 mg/L, Catalyst Dosage = 2.498 g/L and Solution pH = 3)

CHAPTER 5

CONCLUSIONS AND RECOMMENDATIONS

5.1   Conclusions

In this study, pure iron oxide, eggshell particles and iron oxide distributed on eggshell particles were synthesised through green synthesis method by using orange peel was investigated. The green synthesised pure iron oxide, eggshell particles and iron oxide distributed on eggshell particles were characterised by XRD, FTIR, SEM-EDX and TGA. XRD patterns verified that the iron oxide was successfully produced by green synthesis method. FTIR analysis absorption band of pure iron oxide consist of Fe-O bonds while iron oxide distributed on eggshell particles demonstrated bands at 713 cm^{-1} and 873 cm^{-1} which indicated the C-O bond in $CaCO_3$. SEM image showed the morphology of the iron oxide was in spherical shape with average diameter within the range of 0.1 to 1.0 µm. EDX results indicated that Fe, O and C elements were found in pure iron oxide and Fe, O, C and Ca elements were found in iron oxide with eggshell support. TGA analysis for iron oxide distributed on eggshell particles illustrated that the total weight loss was about 37 wt% which contributed to evaporation of water, combustion of inorganic and organic molecules, and phase transformation of iron oxide and decomposition of $CaCO_3$.

The effect of adsorption or photocatalytic degradation on the removal of Congo red had been studied. The photocatalytic degradation efficiency of Congo red by using iron oxide distributed on eggshell particles was higher in the presence of halogen lamp as compared to adsorption process. It was also found that the photocatalytic degradation of Congo red in the presence of eggshell support had improved the catalytic activities of iron oxide. In addition, the catalytic activity of iron oxide and iron oxide supported on eggshell were studied by changing the operating parameters such as initial dye concentration (10-50 ppm), catalyst dosage (0.5-2.5 g/L) and solution pH (3-11). The photocatalytic degradation efficiency of Congo red was increased with decreasing initial dye concentration, increasing catalyst dosage and decreasing solution pH.

On the other hand, optimisation study was conducted by using RSM with CCD model. A polynomial model equation to express the photocatalytic degradation

efficiency in term of initial dye concentration (x_1), catalyst dosage (x_2) and pH value (x_3) had been developed. Based on ANOVA results, the value of R^2 was close to unity which implied that the model was in good agreement with experimental value of photocatalytic degradation efficiency. Besides, the p-value indicated that all terms in the model were significant. For optimisation study, the interaction between three parameters had been determined with response surface diagram. The optimum condition had been generated by RSM where the photocatalytic degradation efficiency of Congo red of 91.32 % were obtained at initial dye concentration of 20.422 mg/L, catalyst dosage of 2.498 g/L and pH of solution of 3.197. The generated optimum condition was verified in the experiment with the efficiency of 92.36 %.

5.2   Recommendations for Future Work

In this study, there was only orange peel extract was used as reducing agent for iron oxide precursor. The types of the fruit peel extracts used as reducing agents should be studied. The amount of fruit peel extract added into the iron solution of $Fe(NO_3)_3 \cdot 9H_2O$ should also be studied. The amount of orange peel extract would affect the amount of iron oxide produced in the solution. Thus, the amount of orange peel extract is an important factor to control the amount of iron oxide produced. Besides, the amount of eggshell added into iron oxide solution is important to enhance the catalytic activity. Eggshell particles acted as support medium for iron oxide particles in order to increase surface area for photocatalytic degradation.

Brunaur-Emmett Teller (BET) surface analysis should be conducted in order to determine the specific surface area of photocatalyst with or without support. Specific surface area is an important factor to affect the photocatalytic degradation efficiency. It is known that higher photocatalytic degradation efficiency could be achieved with higher specific surface area. High contact area would produce high amount of $\cdot OH$. Besides that, inductively coupled plasma - optical emission spectrometry (ICP-OES) analysis should be conducted in order to determine the stability of catalyst. The amount of iron lost into the treated solution would considerably cause toxic effects on human life such as lung cancer and anaemia. Thus, the amount of iron leaching is an important factor to qualify the treated water.

REFERENCES

Abdennouri, M., Baâlala, M., Galadi, A., El Makhfouk, M., Bensitel, M., Nohair, K., Sadiq, M., Boussaoud, A. and Barka, N., 2016. Photocatalytic degradation of pesticides by titanium dioxide and titanium pillared purified clays. *Arabian Journal of Chemistry*, 9, pp. S313–S318.

Adityosulindro, S., 2017. *Activation of homogeneous and heterogeneous Fenton processes by ultrasound and ultraviolet/visible irradiations for the removal of ibuprofen in water*. PhD. University de Toulouse.

Afroz, R. and Rahman, A., 2017. Health impact of river water pollution in Malaysia. *International Journal of Advanced and Applied Sciences*, 4(5), pp. 78–85.

Ahmed, Y., Yaakob, Z. and Akhtar, P., 2016. Degradation and mineralization of methylene blue using a heterogeneous photo-Fenton catalyst under visible and solar light irradiation. *Catalysis Science & Technology*, 6(4), pp. 1222-1232.

Al-Ruqeishi, M. S., Mohiuddin, T. and Al-Saadi, L. K., 2016. Green synthesis of iron oxide nanorods from deciduous Omani mango tree leaves for heavy oil viscosity treatment. *Arabian Journal of Chemistry*.

Ali, A., Zafar, H., Zia, M., Ul Haq, I., Phull, A.R., Ali, J.S. and Hussain, A., 2016. Synthesis, characterization, applications, and challenges of iron oxide nanoparticles. *Nanotechnology, Science and Applications*, 9, pp. 49–67.

Anju Chanu, L., Joychandra Singh, W., Jugeshwar Singh, K. and Nomita Devi, K., 2019. Effect of operational parameters on the photocatalytic degradation of Methylene blue dye solution using manganese doped ZnO nanoparticles. *Results in Physics*, 12, pp. 1230-1237.

Arafat, H. A., 2007. Simple physical treatment for the reuse of wastewater from textile industry in the Middle East. *Journal of Environmental Engineering and Science*, 6(1), pp. 115–122.

Arsalani, S., Guidelli, E. J., Silverira, M.A., Salmon, C. E. G., Araujo, J. F. D. F., Bruno, A. C. and Baffa, O., 2019. Magnetic Fe_3O_4 nanoparticles coated by natural rubber latex as MRI contrast agent. *Journal of Magnetism and Magnetic Materials*, 475, pp. 458-464.

Ayodeji, A. A., Modupe, O. E., Rasheed, B. and Ayodele, J. M., 2018. Data on CaO and eggshell catalysts used for biodiesel production. *Data in Brief*, 19, pp. 1466-1473.

Azbar, N., Yonar, T. and Kestioglu, K., 2004. Comparison of various advanced oxidation processes and chemical treatment methods for COD and color removal from a polyester and acetate fiber dyeing effluent. *Chemosphere*, 55(1), pp. 35–43.

Babuponnusami, A. and Muthukumar, K., 2014. A review on Fenton and improvements to the Fenton process for wastewater treatment. *Journal of Environmental Chemical Engineering*, 2(1), pp. 557–572.

Bacsik, Z., Mink, J. and Keresztury, G., 2004. FTIR spectroscopy of the atmosphere. I. principles and methods. *Applied Spectroscopy Reviews*, 39(3), pp. 295–363.

Barnhert, E.L., Allen, R.M. and Barnhart, E.L., 1993. *The efficacy of color removal techniques in textile wastewater EPRl project manager*.

Bezerra, M. A., Santelli, R. E., Oliveria, E. P., Villar, L. S. and Escaleira, L. A., 2008. Response surface methodology (RSM) as a tool for optimization in analytical chemistry. *Talanta*, 76(5), pp. 965-977.

Bharathi, D., Ranjithkumar, R., Vasantharaj, S., Chandarshekar, B. and Bhuvaneshwari, V., 2019. Synthesis and characterization of chiton/ iron oxide nanocomposite for biomedical applications. *International Journal of Biological Macromolecules*, 132, pp. 880-887.

Bunaciu, A. A., Udriştioiu, E. gabriela and Aboul-Enein, H. Y., 2015. X-Ray Diffraction: instrumentation and applications. *Critical Reviews in Analytical Chemistry*, 45(4), pp. 289–299.

Butler, E., Hung, Y. T., Ahmand, M. A. and Fu, Y. P., 2016. Treatment and management of industrial dye wastewater for water resources. In: Wang, L. K., Wang, M. S., Hung, Y. T. and Shammas, N. K., eds. 2016. *Natural Resources and Control Processes*. Switzerland: Springer Name. pp. 187-232.

Campos, E. A., Stockler Pinto, D. V. B., Oliveira, J. I. S., Mattos, E. D. C. and Dutra, R. D. C. L., 2015. Synthesis, characterization and applications of iron oxide nanoparticles - a short review. *Journal of Aerospace Technology and Management*, 7(3), pp. 267–276.

Chequer, F. M. D., Rodrigues de Oliveira, G.A., Ferraz, E.R.A., Cardoso, J.C., Zanoni, M.V.B. and Palm de Oliveira, D., 2013. Textile dyes : dyeing process and environmental impact. *Eco-friendly Textile Dyeing and Finishing*, pp. 151–176.

Chirayil, C. J., Abraham, J., Mishra, R. K., George, S. C. and Thomas, S., 2017. Instrument techniques for the characterization of nanoparticles. In: Thomas, S., Thomas, R., K.Zachariah, A. and Mishra, R. K., eds. 2017. *Thermal and Rheological Measurement Techniques for Nanomaterials Characterization*. Amsterdam, Netherlands: Elsevier. pp. 1-36.

Coats, A. W. and Redfern, J. P., 1963. Thermogravimetric analysis. *The Analyst*, 88(1053), pp. 906-924.

Deng, Y. and Zhao, R., 2015. Advanced oxidation processes (AOPs) in wastewater treatment. *Current Pollution Reports*, 1(3), pp. 167–176.

Department of Environmental, 2014. *Malaysia environmental quality report 2014.* [online] Available at: <https://enviro.doe.gov.my/ekmc/digital-content/88242/> [Accessed 7 June 2018].

Ebrahimi, R., Maleki, A., Zandsalimi, Y., Ghanbari, R., Shahmoradi, B., Rezaee, R., Safari, M., Joo, S. W., Daraei, H., Harikaranahalli Puttaiah, S. and Giahi, O., 2019. Photocatalytic degradation of organic dyes using WO_3-doped ZnO nanoparticles fixed on a glass surface in aqueous solution. *Journal of Industrial and Engineering Chemistry*, 73, pp. 297-305.

Esmaeilnezhad, E., Karimian, M. and Choi, H. J., 2019. Synthesis and thermal analysis of hydrophobic iron oxide nanoparticles for improving in-situ combustion efficiency of heavy oils. *Journal of Industrial and Engineering Chemistry*, 71, pp. 402-409.

Fang, G.-D., Zhou, D.-M. and Dionysiou, D. D., 2013. Superoxide mediated production of hydroxyl radicals by magnetite nanoparticles: demonstration in the degradation of 2-chlorobiphenyl. *Journal of Hazardous Materials*, 250–251, pp. 68–75.

Fenton, H. J. H., 1894. Oxidation of tartaric acid in presence of iron. *J. Chem. Soc., Trans.*, 65(0), pp. 899–910.

Fontecha-Cámara, M. A., Álvarez-Merino, M.A., Carrasco-Marín, F., López-Ramón, M.V., Moreno-Castilla, C., 2011. Heterogeneous and homogeneous Fenton processes using activated carbon for the removal of the herbicide amitrole from water. *Applied Catalysis B: Environmental*, 101(3–4), pp. 425–430.

Fu, Y., Li, Y., Hu, J. S., Li, S. and Qin, G. W., 2019. Photocatalytic degradation of acetochlor by α-Fe_2O_3 nanoparticles with different morphologies in aqueous solution system. *Optik*, 178, pp. 36-44.

Gaffney, J. S., Marley, N. A. and Jones, D. E., 2012. Fourier transform infrared spectroscopy. In: Kaufmann, E. N., ed. 2012. *Characterization of Materials*. Hoboken, NJ, USA: John Wiley & Sons, Inc. pp. 1104-1135.

Gnanaprakasam, A., Sivakumar, V. M. and Thirumarimurugan, M., 2015. Influencing parameters in the photocatalytic degradation of organic effluent via nanometal oxide catalyst: a review. *Indian Journal of Materials Science*, 2015, pp. 1–16.

Gollakota, A. R. K., Volli, V. and Shu, C. M., 2019. Transesterification of waste cooking oil using pyrolysis residue supported eggshell catalyst. *Science of The Total Environment*, 661, pp. 316-325.

Gopal, S. V., Mini, R., Jothy, V. B. and Joe, I. H., 2015. Synthesis and characterization of iron oxide nanoparticles using DMSO as a stabilizer. *Materials Today: Proceedings*, 2(3), pp. 1051–1055.

Gregory, R. and Edzwald, J. K., 2010. Sedimentation and flotation. In: Edzwald, J. K., ed. 2010. *Water Quality & Treatment: A Handbook on Drinking Water. 6th ed*. New York: American Water Works Association.

Gruskiene, R. Krivorotova, T., Staneviciene, R., Ratautas, D., Serviene, E. and Sereikaite, J., 2018. Preparation and characterization of iron oxide magnetic nanoparticles functionalized by nisin. *Colloids and Surfaces B: Biointerface*s, 169, pp. 126–134.

Guo, L., Chen, F., Fan, X., Cai, W. and Zhang, J., 2010. S-doped α-Fe2O3 as a highly active heterogeneous Fenton-like catalyst towards the degradation of acid orange 7 and phenol. *Applied Catalysis B: Environmental*, 96(1–2), pp. 162–168.

Guo, S., Guo, S., Yuan, N., Zhang, G. and Yu, J.C., 2017. Graphene modified iron sludge derived from homogeneous Fenton process as an efficient heterogeneous Fenton catalyst for degradation of organic pollutants. *Microporous and Mesoporous Materials*, 238, pp. 62–68.

Hassaan, M. A., El Nemr, A. and Madkour, F. F., 2017. Advanced oxidation processes of Mordant Violet 40 dye in freshwater and seawater. *The Egyptian Journal of Aquatic Research*, 43(1), pp. 1–9.

Hassani, A., Karaca, M., Karaca, S., Khataee, A., Açışlı, Ö. and Yılmaz, B., 2018. Preparation of magnetite nanoparticles by high-energy planetary ball mill and its application for ciprofloxacin degradation through heterogeneous Fenton process. *Journal of Environmental Management*, 211, pp. 53–62.

Hassena, H., 2016. Photocatalytic degradation of methylene blue by using Al_2O_3/Fe_2O_3 nano composite under visible light. *Modern Chemistry and Application*, 4(1), p. 1-5.

Hmd, R. F. K., 2011. *Degradation of some textile dyes using biological and physical treatments*. Master. University Ain-Shams.

IHS, 2014. *Epichlorohydrin - Chemical Economics Handbook (CEH) | IHS Markit (2014) IHS Markit.* [online] Available at: <https://ihsmarkit.com/products/dyes-chemical-economics-handbook.html > [Accessed 21 June 2018].

Joshi, M., Bansal, R. and Purwar, R., 2004. Colour removal from textile effluents. *Indian Journal of Fibre and Textile Research*, 29(2), pp. 239–259.

Joshi, M., Bansal, R. and Purwar, R., 2004. Colour removal from textile effluents. *Indian Journal of Fibre and Textile Research*, 29(2), pp. 239–259.

Körlüa, A. E., Yapar, S., Perinçek, S., Yılmaz, H., Bağıran, C., 2015. Dye removal from textile waste water through the adsorption by pumice used in stone washing. *Autex Research Journal*, 15(3), pp. 158–163.

Kadirova, Z. C., Katsumata, K. I., Isobe, T., Matsushita, N., Nakajima, A. and Okada, K., 2013. Adsorption and photodegradation of methylene blue by iron oxide impregnated on granular activated carbons in an oxalate solution. *Applied Surface Science*, 284, pp. 72-79.

Kansara, N., Bhati, L., Narang, M. and Vaishnavi, R., 2016. Wastewater treatment by ion exchange method: a review of past and recent researches. *Environmental Science - An Indian Journal*, 12(4), pp. 143–150.

Karimi, L., Zohoori, S. and Yazdanshenas, M. E., 2014. Photocatalytic degradation of azo dyes in aqueous solutions under UV irradiation using nano-strontium titanate as the nanophotocatalyst. *Journal of Saudi Chemical Society*, 18(5), pp. 581-588.

Kataria, N. and Garg, V. K., 2018. Optimization of Pb (II) and Cd (II) adsorption onto ZnO nanoflowers using central composite design: isotherms and kinetics modelling. *Journal of Molecular Liquids*, 271, pp. 228-239.

Kavitha, V., Geetha, V. and Jacqueline, P. J., 2019. Production of biodiesel from dairy waste scum using eggshell waste. *Process Safety and Environmental Protection*, 125, pp.279-287.

Khatami, M., Alijani, H. Q., Fakheri, B., Mobasseri, M. M., Heydarpour, M., Farahani, Z. K. and Khan, A. U., 2019. Super-paramagnetic iron oxide nanoparticles (SPIONs): Greener synthesis using Stevia plant and evaluation of its antioxidant properties. *Journal of Cleaner Production*, 208, pp. 1171-1177.

Kumar, A. and Pandey, G., 2017. A review on the factors affecting the photocatalytic degradation of hazardous materials. *Material Science & Engineering International Journal*, 1(3).

Laboy-Nieves, E. N., Schaffner, F. C., Abdelhadi, A. H. and Goosen, M. F. A. eds., 2008. *Environmental management, sustainable development and human health*. New York, USA: Taylor & Francis Group, LLC.

Laca, A., Laca, A. and Diaz, M., 2017. Eggshell waste as catalyst: a review. *Journal of Environmental Management*, 197, pp. 351-359.

Lassoued, A., Dkhil, B., Gadri, A. and Ammar, S., 2017. Control of the shape and size of iron oxide (α-Fe_2O_3) nanoparticles synthesized through the chemical precipitation method. *Results in Physics*, pp. 3007–3015.

Leonard, D. N., Chandler, G. W. and Seraphin, S., 2012. Scanning electron microscopy. In: Kaufmann, E. N., ed. 2012. *Characterization of Materials*. Hoboken, NJ, USA: John Wiley & Sons, Inc. pp.1721-1736.

Li, J., Peng, J. H., Guo, S. H and Zhang, L., 2013. Application of response surface methodology (RSM) for optimization of sintering process for the preparation of magnesia partially stabilized zirconia (Mg-PSZ) using natural baddeleyite as starting material. *Ceramics International*, 39(1), pp. 197-202.

Liang, H., Jiang, X., Chen, W., Wang, S., Xu, B. and Wang, Z, 2014. α-Fe_2O_3/Pt hybrid nanorings and their enhanced photocatalytic activities. *Ceramics International*, 40(4), pp.5653-5658.

Ling, J. K. B., 2010. *Water quality study and its relationship with high tide and low tide at Kuantan river*. Degree. University Malaysia Pahang.

Madhura, M. J. and Gayathri, V., 2019. Polymer anchored copper complex as an effective catalyst for photodegradation of organic dyes. *Journal of Photochemistry and Photobiology*.

Majdi, H. Esfahani, J. A. and Mohebbi, M., 2019. Optimization of convective drying by response surface methodology. *Computers and Electronics in Agriculture*, 156, pp.574-584.

Mane, V. S. and Babu, P. V. V., 2011. *Evaluation of performance of Coagulation / Flocculation method for the removal of dyes from aqueous solutions*. Ahmedabad: University Nirma.

Martínez-Cabanas, M., López-García, M., Barriada, J. L., Herrero, R. and Sastre de Vicente, M. E., 2016. Green synthesis of iron oxide nanoparticles. Development of magnetic hybrid materials for efficient As(V) removal. *Chemical Engineering Journal*, 301, pp. 83-91.

Martins, A. C., Cazetta, A. L., Pezoti, O., Souza, J. R. B., Zhang, T., Pilau, E. J., Asefa, T. and Almeida, V. C., 2017. Sol-gel synthesis of new TiO_2 /activated carbon photocatalyst and its application for degradation of tetracycline. *Ceramics Internaltional*, 43(5), pp. 4411-4418.

Mishra, D., Arora, R., Lahiri, S., Amritphale, S.S. and Chandra, N., 2014. Synthesis and characterization of iron oxide nanoparticles by solvothermal method. *Protection of Metals and Physical Chemistry of Surfaces*, 50(5), pp. 628–631.

Mohammad, A., Ahamed, M. I., Amin, A. and Inmuddin, 2017. Removal of nitrogen containing compounds by adsorption: a review. In: Inamuddin and Al-Ahmed, A., eds. 2017. *Applications of Adsorption and Ion Exchange Chromatography in Wastewater Treatment*. Aligrah, India: Materials Research Forum LLC. pp. 44-83.

Mosaddegh, E., Hosseininasab, F. A. and Hassankhani, A., 2015. Eggshell/Fe_3O_4 nanocomposite: novel magnetic nanoparticles coated on porous ceramic eggshell waste as an efficient catalyst in the synthesis of 1,8-dioxo-octahydroxanthene. *RSC Advance,* 5(129), pp.106561-106567.

Muralikrishna, I. V. and Manickam, V., 2017. Wastewater treatment technologies. In: Muralikrishna, I. V., ed. 2017. *Environmental Management*. Oxford: Elsevier.

Nasrollahzadeh, M., Sajadi, S. M. and Hatamifard, A., 2016. Waste chicken eggshell as a natural valuable resource and environmentally benign support for biosynthesis of catalytically active Cu/eggshell, Fe_3O_4/eggshell and Cu/Fe_3O_4/eggshell nanocomposites. *Applied Catalysis B: Environmental*, 191, pp. 209-227.

Nezamzadeh-Ejhieh, A. and Ghanbari-Mobarakeh, Z., 2015. Heterogeneous photodegradation of 2,4-dichlorophenol using FeO doped onto nano-particles of zeolite P. *Journal of Industrial and Engineering Chemistry*, 21, pp. 668-676.

Nikitin, A., Khramtsov, M., Garanina, A., Mogilnikov, P., Sviridenkova, N., Shchetinin, I., Savchenko, A., Abakumov, M. and Majouga, A., 2019. Synthesis of iron oxide nanorods for enhanced magnetic hyperthermia. *Journal of Magnetism and Magnetic Materials*, 469, pp. 443-449.

Pandey, A., Kalal, S., Salvi, N., Ameta, C., Ameta, R. and Punjabi, P.B., 2018. Preparation, characterization and applications of visible light responsive photocatalytic materials. In: Tayade, R. J. and Gandhi, V., eds. 2018. *Photocatalytic Nanomaterials for Environmental Applications*. Millersville, USA: Materials Research Forum LLC.

Pang, Y. L., Abdullah, A. Z. and Bhatia, S., 2011. Optimization of sonocatalytic degradation of Rhodamine B in aqueous solution in the presence of TiO_2 nanotubes using response surface methodology. *Chemical Engineering Journal*, 166(3), pp. 873-880.

Pang, Y. L., Lim, S., Ong, H. L. and Chong, W.T., 2015. Research progress on iron oxide-based magnetic materials: synthesis techniques and photocatalytic applications. *Ceramics International*, 42, pp. 9–34.

Pignatello, J. J., Oliveros, E. and MacKay, A., 2006. Advanced oxidation processes for organic contaminant destruction based on the Fenton reaction and related chemistry. *Critical Reviews in Environmental Science and Technology*, 36(1), pp. 1–84.

Pouretedal, H. R., Norozi, A., Keshavarz, M. H. and Semnani, A., 2009. Nanoparticles of zinc sulfide doped with manganese, nickel and copper as nanophotocatalyst in the degradation of organic dyes. *Journal of Hazardous Materials¸*162(2), pp. 674-681.

Prodan, A. M., Iconaru, S. L., Ciobanu, C. S., Chifiriuc, M. C., Stoicea, M. and Predoi, D., 2013. Iron oxide magnetic nanoparticles: characterization and toxicity evaluation by In Vitro and In Vivo assays. *Journal of Nanomaterials*, 2013, pp. 1–10.

Quader, A. K. M. A., 2010. Treatment of textile wastewater with chlorine: an effective method. *Chemical Engineering Research Bulleti*n, 14(1), pp. 59–63.

Radu, T., Iacovita, C., Benea, D. and Turcu, R., 2017. X-ray photoelectron spectroscopic characterisation of iron oxide nanoparticles. *Applied Surface Science*, 405, pp. 337-343.

Rajamanickam, D. and Shanthi, M., 2016. Photocatalytic degradation of an organic pollutant by zinc oxide – solar process. *Arabian Journal of Chemistry*, 9, pp. S1858–S1868.

Rajiv, P., Bavadharani, B., Kumar, M. N. and Vanathi, P., 2017. Synthesis and characterization of biogenic iron oxide nanoparticles using green chemistry approach and evaluating their biological activities. *Biocatalysis and Agricultural Biotechnology*, 12, pp. 45-49.

Reza, K. M., Kurny, A. and Gulshan, F., 2017. Parameters affecting the photocatalytic degradation of dyes using TiO_2: a review. *Applied Water Science*, 7(4), pp. 1569–1578.

Ribeiro, A. R., Nunes, O. C., Pereira, M. F. R. and Silva, A. M. T., 2015. An overview on the advanced oxidation processes applied for the treatment of water pollutants defined in the recently launched Directive 2013/39/EU. *Environment International*. Pergamon, pp. 33–51.

Rossi, A. F., 2014. *Fenton's process applied to wastewaters treatment*. PhD. University of Coimbra.

Ruíz-Baltazar, A. J., Reyes-López, S. Y., Mondragón-Sánchez, M. L., Robles-Cortés, A. I. and Pérez, R., 2019. Eco-friendly synthesis of Fe_3O_4 nanoparticles: Evaluation of their catalytic activity in methylene blue degradation by kinetic adsorption models. *Results in Physics*, 12, pp. 989-995.

Samer, M., 2015. Biological and chemical wastewater treatment processes. *Wastewater Treatment Engineering*, pp. 1–50.

Santos, C. M., Dweck, J., Viotto, R. S., Rosa, A. H. and Morais, L. C., 2015. Application of orange peel waste in the production of solid biofuels and biosorbents. *Bioresource Technology*, 196, pp. 469-479.

Saqib Nawaz, M. and Ahsan, M., 2014. Comparison of physico-chemical, advanced oxidation and biological techniques for the textile wastewater treatment. *Alexandria Engineering Journal*, 53, 717-722.

Saratale, R. G., Noh, H. S., Song, J. Y. and Kim, D. S., 2014. Influence of parameters on the photocatalytic degradation of phenolic contaminants in wastewater using TiO_2/UV system. *Journal of Environmental Science and Health*, 49(13), pp. 1542–1552.

Saravanan, R., Gracia, F. and Stephen, A., 2017. Basic Principles, Mechanism, and Challenges of Photocatalysis. In: K. M. Mohamad, P. Debabrata and S. Youngku, eds. 2017. *Nanocomposites for visible light-induced photocatalysis*. Switzerland: Springer International. pp. 19-40.

Shi, X. G., Tian, A., You, J. H., Yang, H., Wang, Y. Z. and Xue, X. X., 2018. Degradation of organic dyes by a new heterogeneous Fenton reagent - Fe_2GeS_4 nanoparticle. *Journal of Hazardous Materials*, 353, pp.182-189.

Si, L., Yang, W., Cao, C., Wang, Y. and Yang, S., 2013. Research progress of the physical and chemical treatment of dye wastewater. *International Journal of Scientific & Engineering Research*, 4(5).

Siriprom, W., Sangwaranatee, N., Hidayat, R., Kongsriprapan, S., Teanchai, K. and Chamchoi, N., 2018. The physicochemical characteristic of biodegradable methylcellulose film reinforced with chicken eggshells. *Materials Today: Proceedings*, 5(7), pp. 14836-14839.

Sktani, Z. D. I., Rejab, N. A., Ratnam, M. M. and Ahmad, Z. A., 2018. Fabrication of tougher ZTA ceramics with sustainable high hardness through (RSM) optimisation. *International Journal of Refractory Metals and Hard Materials*, 74, pp. 78-86.

Solanki, M., Suresh, S., Das, S. N. and Shukla, K., 2013. Treatment of real textile wastewater using coagulation technology. *International Journal of ChemTech Research*, 5(2), pp. 974–4290.

Song, C. J., Li, X. Y., Wang, L. P. and Shi, W. D., 2016. Fabrication, Characterization and Response Surface Method (RSM) Optimization for Tetracycline Photodegration by $Bi_{3.84}W_{0.16}O_{6.24}$- graphene oxide (BWO-GO). *Scientific Reports*, 6(1).

Sreeja, P. H. and Sosamony, K. J., 2016. A comparative study of homogeneous and heterogeneous photo-Fenton process for textile wastewater treatment. *Procedia Technology*, 24, pp. 217–223.

Stokes, D. J., 2008. Principle of SEM. In: Rainforth, M., ed. *Principles and practice of variable pressure/environmental scanning electron microscopy*. Chichester, UK: John Wiley & Sons, Ltd. pp.17-62.

Subashini, L. M., 2015. Review on biological treatment process of pulp and paper industry waste water. *International Journal of Innovative Research in Science, Engineering and Technology*, 4(5), pp.3721-3725.

Sulaiman, N., Ida Idayu, M., Ramlan, A., Nor Farahiyah, A. N., Taher, Z. M., Nor Rashidah, A. and Mohamad, M. F., 2019. Enhancement of gaharu oleoresin quality by process optimization using response surface methodology. *Biocatalyst and Agricultural Biotechnology*, 18, pp. 101066-101074.

Sun, Y., Yang, Y., Yang, M., Yu, F. and Ma, J., 2019. Response surface methodological evaluation and optimization for adsorption removal of ciprofloxacin onto graphene hydrogel. *Journal of Molecular Liquids*.

Teja, A. S. and Koh, P.-Y., 2009. Synthesis, properties, and applications of magnetic iron oxide nanoparticles. *Progress in Crystal Growth and Characterization of Materials*, 55(1–2), pp. 22–45.

Textile Design and Fashion Art, 2012. *Dyes | Classification Of Dyes | Textile Fashion Study*. [online] Available at: <http://textilefashionstudy.com/dyes-classification-of-dyes/> [Accessed: 21 June 2018].

Thermo Nicolet Corporation, 2015. Introduction to fourier transform infrared spectrometry. Madison, USA: Thermo Nicolet Corporation.

Tsai, W. T., Hsien, K. J., Hsu, H. C., Lin, C. M., Lin, K. Y. and Chiu, C. H., 2008. Utilization of ground eggshell waste as an adsorbent for the removal of dyes from aqueous solution. *Bioresource Technology*, 99(6), pp. 1623-1629.

Upadhye, V. B. and Joshi, S. S., 2012. Advances in wasterwater treatment - a review. *International Journal of Chemical Sciences and Applications*, 3(2), pp. 2278–6015.

Vyazovkin, S., 2012. Thermogravimetric analysis. In: Kaufmann, E. N., ed. 2012. *Characterization of Materials*. Hoboken, NJ, USA: John Wiley & Sons, Inc.

Warkhade, S. K., Zodape, S. P., Pratap, U. R. and Wankhade, A. V., 2019. Rutile TiO_2/CoSe nanocomposite: An efficient photocatalyst for photodegradation of model organic dyes under visible light irradiation. *Journal of Molecular Liquids¸* 279, pp. 434-443.

Wei, Y., Han, B., Hu, X. Y., Lin, Y. H., Wang, X. Z. and Deng, X. L., 2012. Synthesis of Fe_3O_4 nanoparticles and their magnetic properties. *Procedia Engineering*, 27, pp. 632-637.

Wu, W., He, Q. and Jiang, C., 2008. Magnetic iron oxide nanoparticles: synthesis and surface functionalization strategies. *Nanoscale Research Letters*, 3(11), pp. 397-415.

Wu, W., Wu, Z., Yu, T., Jiang, C. and Kim, W., 2015. Recent progress on magnetic iron oxide nanoparticles: synthesis, surface functional strategies and biomedical applications. *Science and Technology of Advanced Material*, 16(2), p. 023501.

Xavier, S., Gandhimathi, R., Nidheesh, P. V. and Ramesh, S. T., 2015. Comparison of homogeneous and heterogeneous Fenton processes for the removal of reactive dye Magenta MB from aqueous solution. *Desalination and Water Treatment*, 53(1), pp. 109–118.

Xu, C., Rangaiah, G. P. and Zhao, X. S., 2014. Photocatalytic degradation of methylene blue by titanium dioxide: experimental and modeling study. *Industrial & Engineering Chemistry Research*, 53(38), pp. 14641–14649.

Xu, P., Zeng, G. M., Huang, D. L., Feng, C. L., Hu, S., Zhao, M. H., Lai, C., Wei, Z., Huang, C., Xie, G.X. and Liu, Z.F., 2012. Use of iron oxide nanomaterials in wastewater treatment: a review. *Science of The Total Environment*, 424, pp. 1–10.

Yadav, M., 2018. Study on thermal and mechanical properties of cellulose/iron oxide bionanocomposites film. *Composites Communications*, 10, pp. 1-5.

Yusuf, M., Shabbir, M. and Mohammad, F., 2017. Natural colorants: historical, processing and sustainable prospects. *Natural Products and Bioprospecting*, 7(1), pp.123-145.

Zaera, F. and Ma, Z., 2006. *Surface and Nanomolecular Catalysis*. CRC Press, pp. 1–38.

Zhang, X., Wu, F., Wu, X. W., Chen, P. Y. and Deng, N. S., 2008. Photodegradation of acetaminophen in TiO_2 suspended solution. *Journal of Hazardous Materials*, 157(2), pp. 300-307.

APPENDICES

APPENDIX A: Preparation of Various Concentrations of Congo red

The concentration of Congo red that required for experiment is obtained from a stock solution through dilution with distilled water. The volume from stock solution that is required can be computed by using equation (A1) with those known parameters such as the concentration of stock solution, desired concentration of organic dye and volume of organic dye.

$$C_1 V_1 = C_2 V_2 \qquad\qquad (A1)$$

where

C_1 = the concentration of stock solution, g/L

V_1 = the volume of stock solution, L

C_2 = the final concentration of diluted solution, g/L

V_1 = the final volume of diluted solution, L

The value of V_1 is determined by using equation (A1). After that, volume of V_1 of stock solution is pipetted and then it is diluted by adding distilled water until the volume of diluted solution equal to V_2.

To prepare the stock solution of 40% of Congo red with concentration of 1000 ppm in 200 mL, the mass of Congo red powder required is computed as below:

$$
\begin{aligned}
Mass\ of\ Congo\ Red,\quad m \quad &= \quad \frac{1}{0.40} \times 1000\ \frac{mg}{L} \times 0.2L \\
&= \quad 500\ mg \\
&= \quad 0.5\ g
\end{aligned}
$$

To prepare a stock solution with concentration of 1000 ppm of Congo red in 250 mL, 0.5 g of Congo red powder is required to dissolve in 250 mL of distilled water.

To prepare different dye concentration that less than 1000 ppm from volume of 40% Congo red stock solution with 1000 ppm is determined as below. For example, to prepare 100 ml of diluted Congo red solution with concentration of 20 ppm, the volume required of stock solution is calculated as below:

$$(1000 \ mg/L)(V_1) = (20 \ mg/L)(100 \ ml)$$
$$V_1 = 2 \ ml$$

Therefore, 2 ml of Congo red stock solution is added into 98 ml of distilled water to obtained 20 ppm of diluted Congo red solution.

Table A-1: The Volume of Congo Red Stock Solution Required to Prepare Certain Concentration of Congo Red in 100 ml Solution

Concentration of Congo Red (mg/L)	Volume of Congo Red Stock Solution with 1000 ppm Required (mL)
10	1
20	2
30	3
40	4
50	5

APPENDIX B: Preparation of 0.1 M HCl from 37% HCl

Molarity of 37 % HCl

HCl, 37% v/v = 37 mL/ 100mL

Specific gravity of 37 % HCl = 1.19 g/ml

Molecular weight of HCl = 36.46 g/mol

$$Concentration\ of\ HCl\ in\ g/L \quad = \quad \frac{37\ ml}{100\ ml} \times \frac{1.19\ g}{ml}$$

$$= \quad \frac{0.4403 g}{ml} \times \frac{1000\ ml}{1\ L}$$

$$= \quad 440.3\ g/L$$

$$Molarity\ of\ HCl \quad = \quad \frac{440.3\ g}{L} \times \frac{mol}{36.46\ g}$$

$$12.07\ mol/L$$

The volume of 37 % HCl required for 0.1 M HCl solution is computed by using equation (A2)

$$M_1 V_1 = M_2 V_2 \qquad\qquad (A1)$$

where

M_1 = the concentration of 37 % HCl solution, mol/L

V_1 = the volume of 37 % HCl solution, L

M_2 = the final concentration of diluted HCl solution, mol/L

V_2 = the final volume of diluted HCl solution, L

$$M_1 = 12.07\ M, M_2 = 0.1\ M, V_2 = 500\ mL$$

$$V_1 \quad = \quad \frac{M_2 V_2}{M_1}$$

$$= \quad \frac{0.1\ M \times 500\ ml}{12.07\ M}$$

$$= \quad 4.14\ ml$$

Therefore, the volume of 37 % HCl is required to added is 4.14 ml to obtain 0.1 M of HCl solution with volume of 500 mL.

APPENDIX C: Preparation of 0.1 M NaOH from 97% NaOH

The mass of NaOH pellet required to prepare 0.1 M of NaOH in 500 ml is determined as below:

$$Number\ of\ moles\ of\ NaOH\ =\ Molarity\left(\frac{mol}{L}\right) \times Volume(L) \times purity$$

$$=\ 0.1\ mol/L \times 500\ ml \times \frac{1L}{1000\ mL} \times \frac{100}{97}$$

$$=\ 0.052\ moles$$

The molecular weight of NaOH = 40 g/mol,

$$Mass\ of\ NaOH\ =\ Moles_{NaOH} \times MW_{NaOH}$$

$$=\ 0.052\ moles \times 40\ g/mol$$

$$=\ 2.08\ g$$

Therefore, the mass of NaOH pellet is required to add is 2.08 g to obtain 0.1 M of HCl solution with volume of 500 mL.
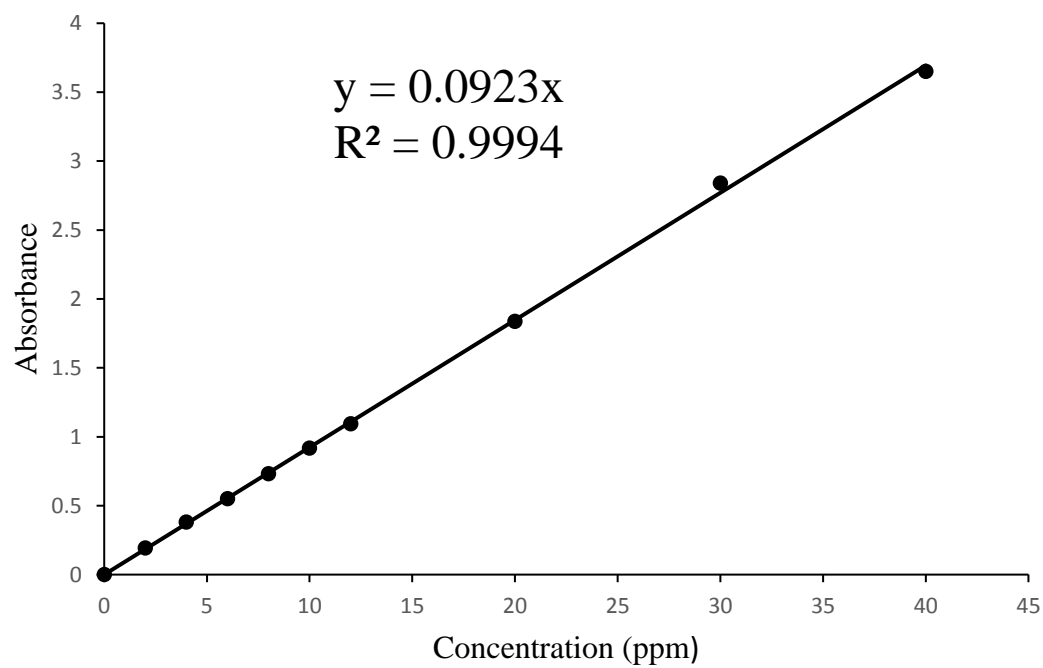
APPENDIX D: Calibration Curve of Organic Dyes

Figure D-1: Calibration Curve of Congo Red

APPENDIX E: Calculation of Crystalline Size

The crystalline size of materials can be calculated from XRD pattern using the Scherrer equation (Lassoued, et al., 2017)

$$D_c = \frac{K\lambda}{\beta cos\theta} \tag{2.23}$$

where

K = shape factor, 0.9

λ = the wavelength of the X-rays, (0.15148nm for CuK$_\alpha$)

β = the full width at half maximum

θ = the diffraction angle

Peak data for iron oxide nanoparticles without eggshell support:

β = 0.16230°

θ = 29.3737°

$$
\begin{aligned}
D_1 &= \frac{K\lambda}{\beta cos\theta} \\
&= \frac{0.90 \times 1.5148}{\left(0.16230 \times \frac{\pi}{180}\right)cos(\frac{29.3737}{2})} \\
&= 497.541 \text{ Å} \\
&= 49.75 \, nm
\end{aligned}
$$

Peak data for iron oxide nanoparticles with eggshell support:

β = 0.14400°

θ = 29.4081°

$$
\begin{aligned}
D_2 &= \frac{K\lambda}{\beta cos\theta} \\
&= \frac{0.90 \times 1.5148}{\left(0.1440 \times \frac{\pi}{180}\right)cos(\frac{29.4081}{2})} \\
&= 560.81 \text{ Å} \\
&= 56.08 \, nm
\end{aligned}
$$